A spatialized model of textures perception using structure tensor formalism

Grégory Faye, Pascal Chossat

Manuscript submitted to
AIMS' Journals
Volume **X**, Number **0X**, XX **200X**

Website: http://AIMsciences.org

pp. **X–XX**

A SPATIALIZED MODEL OF VISUAL TEXTURE PERCEPTION USING THE STRUCTURE TENSOR FORMALISM

Grégory Faye

School of Mathematics, University of Minnesota
206 Church Street S.E., Minneapolis, MN 55455, USA
and
Neuromathcomp Project Team, INRIA Sophia Antipolis
2004 Route des Lucioles, F-06902 Sophia Antipolis

Pascal Chossat

J-A Dieudonné Laboratory, CNRS and University of Nice Sophia-Antipolis
Parc Valrose, 06108 Nice Cedex 02, France
and
Neuromathcomp Project Team, INRIA Sophia Antipolis

(Communicated by the associate editor name)

Abstract. The primary visual cortex (V1) can be partitioned into fundamental domains or hypercolumns consisting of one set of orientation columns arranged around a singularity or "pinwheel" in the orientation preference map. A recent study on the specific problem of visual textures perception suggested that textures may be represented at the population level in the cortex as a second-order tensor, the structure tensor, within a hypercolumn. In this paper, we present a mathematical analysis of such interacting hypercolumns that takes into account the functional geometry of local and lateral connections. The geometry of the hypercolumn is identified with that of the Poincaré disk $\mathbb{D}$. Using the symmetry properties of the connections, we investigate the spontaneous formation of cortical activity patterns. These states are characterized by tuned responses in the feature space, which are doubly-periodically distributed across the cortex.

1. **Introduction.** The formation of steady state patterns through Turing mechanism is a well-known phenomenon [50, 33]. For example, it occurs when a homogeneous state of a system of reaction-diffusion equations defined on the Euclidean plane becomes neutrally stable when a bifurcation parameter reaches a critical value. For the analysis of this phenomenon, the assumption that the system is invariant under Euclidean transformations in the plane is essential. Any Fourier mode whose wave vector has critical length is a neutral stable mode and a consequence of the rotational symmetry of the system is that the kernel of linearized problem at the bifurcation point is infinite dimensional. By looking at the class of $\mathcal{L}$-periodic states, $\mathcal{L}$ being a discrete translation subgroup of $\mathbb{R}^2$, or by looking at the system projected onto the torus $\mathbb{R}^2/\mathcal{L}$, one renders the spectrum of the linearized problem discrete:

2000 *Mathematics Subject Classification.* Primary: 37G40, 34C23; Secondary: 92B20.

Key words and phrases. Neural field equations, symmetry, equivariant bifurcation, pattern formation, Poincaré disk.

This work was partially funded by the ERC advanced grant NerVi number 227747.

the critical wave vectors are finite in number, hence the critical eigenvalue has finite multiplicity and standard methods of equivariant bifurcation theory (see [19, 29]) can be applied to compute bifurcated solutions within the class of $\mathcal{L}$-periodic states. Such solutions are called *planforms*.

Ermentrout and Cowan [25] were first to propose a mathematical theory of visual patterns seen during hallucinations. Hallucinations can occur in a wide variety of situations such as with migraine headaches, epilepsy or as the result of external stimulus by drugs such as LSD [41, 52]. In their model, the visual cortex is idealized by the Euclidean plane and it is assumed that the effect of drugs is to cause instabilities, by spontaneous symmetry- breaking, in the neural activity and these instabilities result in the visual patterns experienced by the subjects. This model assumes that neurons in the visual cortex are not sensitive to features such as orientation, texture, color etc.

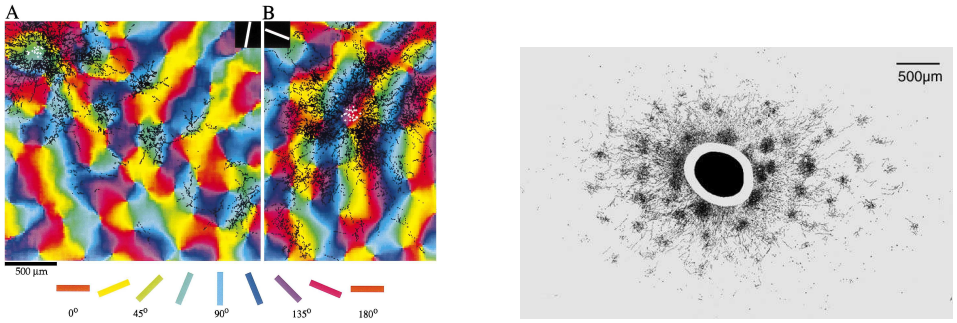

(a) Redrawn from Bosking et al [8].

(b) Redrawn from Lund et al [46].

FIGURE 1. Lateral connections made by V1 cells in Tree Shrew (left) and Macaque (right). A radioactive tracer is used to show the locations of all terminating axons from cells in a central injection site, superimposed on an orientation map obtained by optical imaging.

However it has been well documented that neurons in the primary visual cortex respond preferentially to visual stimuli that have a specific orientation. Subgroups of inhibitory and excitatory neurons are tuned to a particular orientation of an external stimulus, form what is called a *Hubel and Wiesel hypercolumn* of the visual area V1 in the cortex (roughly 1 mm^2 of cortical surface) [34, 35, 36]. Two cortical circuits have been characterised which further manifest the functional structure of V1. A local circuit, operating at sub-hypercolumn dimensions, consists of a mixture of intra-cortical excitation and inhibition. Such circuit provides a substrate for the recurrent amplification and sharpening of the tuned response of cells to local visual stimuli (for example the ring model of orientation where the inhibitory connections are more broadly tuned with respect to orientation than the excitatory connections [4, 30]). A lateral circuit, operating between hypercolumns, anisotropically connects cells with similar functional properties: cells in different hypercolumns tend to connect in directions parallel to their common preferred orientation (see figures 1(a) and 1(b)). Based on these anatomical structures, Bressloff et al [14, 12] took into account the orientation of cortical neurons and abstracted the visual cortex as $\mathbb{R}^2 \times \mathbf{S}^1$. Their analysis recovered thin line hallucinations such as cobwebs and

honeycombs. However, the anisotropic nature of cortical long-range connections can be weak upon species. For macaques (see figure 1(b)) anisotropy tends to be weaker than for tree shrews (see figure 1(a)). This remark has been incorporated into numerous models of cortical map development [69, 39, 38]. Following this idea, Golubitsky et al [28] revisited the model of Bressloff et al [14, 12] by determining solutions obtained from symmetry-breaking bifurcations in the case of isotropic lateral coupling and then studying how these solutions may change when anisotropy is introduced as a forced symmetry-breaking parameter.

Neurons in the visual cortex not only respond preferentially to visual stimuli that have a specific orientation but also to spatial frequency [10], velocity and direction of motion [51], color [35]. Chossat and Faugeras have introduced in [20] a new approach to model the processing of image edges and textures in the hypercolumns of V1 that is based on a nonlinear representation of the image first order derivatives called the structure tensor [5, 42]. It was suggested that this structure tensor was represented by neuronal populations in the hypercolumns of V1 and that the time evolution of this representation was governed by equations similar to those proposed by Wilson and Cowan [67]. By definition, the structure tensor is based on the spatial derivatives of an image in a small area that can be thought of as part of a receptive field. These spatial derivatives are then summed nonlinearly over the receptive field. Let $I(x, y)$ denote the original image intensity function, where x and y are two spatial coordinates. Let I^{σ_1} denote the scale-space representation of I obtained by convolution with the Gaussian kernel $g_\sigma(x, y) = \frac{1}{2\pi\sigma^2} e^{-\frac{x^2+y^2}{2\sigma^2}}$:

$$I^{\sigma_1} = I \star g_{\sigma_1}.$$

The gradient ∇I^{σ_1} is a two-dimensional vector of coordinates $I_x^{\sigma_1}$, $I_y^{\sigma_1}$ which emphasizes image edges. One then forms the 2×2 symmetric matrix of rank one $\mathcal{T}_0 = \nabla I^{\sigma_1} (\nabla I^{\sigma_1})^{\mathbf{T}}$, where $^{\mathbf{T}}$ indicates the transpose of a vector. By convolving $\mathcal{T}_0$ componentwise with a Gaussian function g_{σ_2} we finally form the tensor structure as the symmetric matrix:

$$\mathcal{T} = \mathcal{T}_0 \star g_{\sigma_2} = \begin{pmatrix} \langle (I_x^{\sigma_1})^2 \rangle_{\sigma_2} & \langle I_x^{\sigma_1} I_y^{\sigma_1} \rangle_{\sigma_2} \\ \langle I_x^{\sigma_1} I_y^{\sigma_1} \rangle_{\sigma_2} & \langle (I_y^{\sigma_1})^2 \rangle_{\sigma_2} \end{pmatrix}$$

where we have set for example:

$$\langle (I_x^{\sigma_1})^2 \rangle_{\sigma_2} = (I_x^{\sigma_1})^2 \star g_{\sigma_2}.$$

Since the computation of derivatives usually involves a stage of scale-space smoothing, the definition of the structure tensor requires two scale parameters. The first one, defined by σ_1, is a local scale for smoothing prior to the computation of image derivatives. The structure tensor is insensitive to noise and details at scales smaller than σ_1. The second one, defined by σ_2, is an integration scale for accumulating the nonlinear operations on the derivatives into an integrated image descriptor. It is related to the characteristic size of the texture to be represented, and to the size of the receptive fields of the neurons that may represent the structure tensor.

The question of whether some populations of neurons in such a visual area as V1 can represent the structure tensor cannot be answered at this point in a definite manner and is still an open question. At the stage of this paper we can nonetheless argue as follows. Cytochrome oxydase (CO) blobs and their neighborhoods seem good candidates since their distribution appears to be correlated with a number of periodically repeating feature maps in which local populations of neurons respond

preferentially to stimuli with particular properties such as orientation, spatial frequency, brightness and contrast. It has thus been suggested that the CO blobs could be the sites of functionally and anatomically distinct channels of visual processing [23, 45, 61, 63]. Bressloff and Cowan [10, 9] introduced a model of a hypercolumn in V1 consisting of orientation and spatial frequency preferences organized around a pair of pinwheels. One pinwheel is centered at a CO blob and encodes coarse to medium coarse scales, the other is centered at a region that encodes medium coarse to fine scales. Such a hypercolumn is therefore a good candidate for representing the structure tensor at several scales as well as the local orientations at various spatial frequencies. Finally, it was shown in very recent study [44] that neurons selective to the direction of motion preferentially fire for natural-like random textures which seems to corroborate the hypothesis that there exists neurons in the visual cortex coding for textures.
This is one aim of the present work to allow for predictions about the kinds of patterns that should be observed in the activity of real brains. This would open the door to the design of experiments to test and probe the neurophysiological hypotheses of the structure tensor model.

In previous studies [20, 27, 18, 26] we explored the bifurcation of patterns within a single hypercolumn of structure tensors. For the spatial problem, this comes back to assume that the hypercolumns are independent form each other. This was a first and necessary step before spatialization.

Our aim is now at introducing lateral connections in the structure tensor model and analyzing the bifurcation of patterns for this spatialized model. The visual cortex is now abstracted as $\mathbb{R}^2 \times \mathbf{SPD}(2,\mathbb{R})$, where the feature space $\mathbf{SPD}(2,\mathbb{R})$ is the set of all structure tensors, that is the set of 2×2 symmetric positive definite matrices. We shall see in the next section that $\mathbf{SPD}(2,\mathbb{R})$ is an unbounded Riemann space, namely the solid cone equipped with a suitable metric. As shown in [20, 27], the neurons within a hypercolumn are connected to each others with a weight depending on the structure tensors that these neurons encode. Moreover, it is natural to assume that these connections are invariant under the action of the group of isometries of the Riemann space $\mathbf{SPD}(2,\mathbb{R})$, namely the unbounded Lie group $\mathbf{GL}(2,\mathbb{R})$.

It is important to mention here the neurogeometric approach developed by Petitot, Sarti and Citti [22, 58, 54, 55]. The idea behind neurogeometry is to model the functional architecture of the primary visual cortex as a principal fiber bundle where the two-dimensional retinal plane is the base manifold $\mathbb{R}^2$ and all the secondary variables like orientation, spatial frequency, color, texture constitute the fibers over each point. For example in the case of orientation and spatial frequency, Sarti, Citti and Petitot have shown that the total space is endowed with a simplectic structure neurally implemented by long range horizontal connections [58]. In particular, this neuro-geometrical approach has proven its efficiency for image completion problems [54, 22, 56]. However, as we are interested in the study of the different types of cortical states that can be spontaneously produced by our spatialized model and then interpret them as geometric visual hallucinations, we did not pursue in that direction and we will rather use a symmetry-breaking bifurcation analysis approach throughout this paper.

The unboundedness of the isometry group $\mathbf{GL}(2,\mathbb{R})$ introduces an important complication in the bifurcation analysis compared to the ring model of orientation

preferences. We shall see in Section 2 that two different approaches can be followed in order to overcome this difficulty. One is to remark that in a "real" cortex an upper bound must exist to the norm of effectively detectable structure tensors, and therefore consider a suitably chosen bounded domain in $\mathbf{SPD}(2,\mathbb{R})$ instead of $\mathbf{SPD}(2,\mathbb{R})$ itself. The other is to take advantage of the previous analysis presented in [18] where the bifurcation of periodic patterns in $\mathbf{SPD}(2,\mathbb{R})$ was investigated. Periodic means here that the patterns are invariant under the action of a discrete subgroup L of $\mathbf{GL}(2,\mathbb{R})$ which tiles the space $\mathbf{SPD}(2,\mathbb{R})$ with a compact fundamental domain. This method allows to reduce the domain to the quotient space $\mathbf{SPD}(2,\mathbb{R})/L$, which is a compact manifold.
These two approaches are investigated respectively in Sections 3 and 4. In fact, as explained in Section 2, it is possible to work with the hyperbolic plane (identified further with the Poincaré disk) instead of the cone $\mathbf{SPD}(2,\mathbb{R})$. This will introduce an additional, however unessential, simplification.

2. The continuum models of V1 and their symmetries.

2.1. **The model equations.** The average membrane potential of a population of neurons at a cortical position $\mathbf{r} \in \mathbb{R}^2$ at time t is characterized by the real valued function $V(\mathbf{r},\mathcal{T},t)$, where $\mathbf{r}$ labels a point in the visual cortex and $\mathcal{T}$ is a structure tensor. All possible textures are represented at every position: $\mathbf{r}$ and $\mathcal{T}$ are independent variables. The average membrane potential evolves according to a generalization of the Wilson-Cowan equations [68]:

$$\frac{\partial V(\mathbf{r},\mathcal{T},t)}{\partial t} = -V(\mathbf{r},\mathcal{T},t) + \int_{\mathbb{R}^2}\int_{\mathbf{SPD}(2,\mathbb{R})} W(\mathbf{r},\mathcal{T} \mid \mathbf{r}',\mathcal{T}')S(\mu V(\mathbf{r}',\mathcal{T}',t))d\mathcal{T}'d\mathbf{r}'. \tag{2.1}$$

Note that we put no external input in this equation, meaning that we look at *spontaneous pattern formation*. The nonlinearity S is a smooth sigmoidal function which saturates at $\pm\infty$ with $S(0) = 0$. In order to fix ideas we work with the following sigmoidal function:

$$S(x) = \frac{1}{1+e^{-x+T}} - \frac{1}{1+e^{T}}, \tag{2.2}$$

where T is a positive threshold. The parameter μ describes the stiffness of the sigmoid.
With this nonlinearity, $V = 0$ is always solution.

The associated weight distribution is decomposed into local (within the hypercolumns) and long-range parts according to:

$$W(\mathbf{r},\mathcal{T} \mid \mathbf{r}',\mathcal{T}') = W_{loc}(d_{\mathbf{SPD}(2,\mathbb{R})}(\mathcal{T},\mathcal{T}'))\delta_{\mathbf{r},\mathbf{r}'} + \beta(1-\delta_{\mathbf{r},\mathbf{r}'})W^{\epsilon}_{lat}(\mathbf{r},\mathcal{T} \mid \mathbf{r}',\mathcal{T}'). \tag{2.3}$$

We normalize the total weight of both local and long-range connections:

$$\int_{\mathbf{SPD}(2,\mathbb{R})} W_{loc}(d(\mathcal{T},\mathcal{T}'))d\mathcal{T}' = 1$$
$$\int_{\mathbb{R}^2}\int_{\mathbf{SPD}(2,\mathbb{R})} W^{\epsilon}_{lat}(\mathbf{r},\mathcal{T} \mid \mathbf{r}',\mathcal{T}')d\mathcal{T}'d\mathbf{r}' = 1.$$

Microelectrode recordings suggest that β is small and therefore that the lateral connections modulate rather than drive the cortical activity. The sign of β will

determine whether the lateral connections have a net excitatory or inhibitory effect. The rules of long-range connections are given by:

$$W^{\epsilon}_{lat}(\mathbf{r},\mathcal{T}\mid\mathbf{r}',\mathcal{T}')=\mathcal{J}\left(\sqrt{(\mathbf{r}-\mathbf{r}')^{\mathbf{T}}(\mathbf{I}_2+\epsilon\mathcal{T})(\mathbf{r}-\mathbf{r}')}\right)\mathcal{K}\left(d\left(\mathcal{T},\mathcal{T}'\right)\right) \tag{2.4}$$

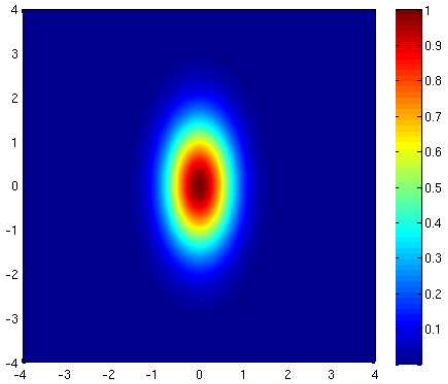

FIGURE 2. Plot of $\mathbf{r}\to\mathcal{J}\left(\sqrt{\mathbf{r}^{\mathbf{T}}(\mathbf{I}_2+\epsilon\mathcal{T})\mathbf{r}}\right)$ in the definition of long-range connections. $\mathcal{N}=\xi=1$, $\epsilon=0.05$ and $\mathcal{T}=\mathrm{diag}\,(50,0.2)$.

The first factor $\mathcal{J}$ incorporates the observation that the density patches tends to decrease monotonically with cortical separation and lies along the direction of their feature preference. For definiteness, we take $\mathcal{J}$ to be a Gaussian $\mathcal{J}(x)=\mathcal{N}e^{-x^2/2\xi^2}$. For an illustration purpose, in figure 2, we plot the profile of $\mathbf{r}\to\mathcal{J}\left(\sqrt{\mathbf{r}^{\mathbf{T}}(\mathbf{I}_2+\epsilon\mathcal{T})\mathbf{r}}\right)$, for specific values of the parameters and a diagonal structure tensor $\mathcal{T}=\mathrm{diag}(50,0.2)$ which has a preferred orientation at $\frac{\pi}{2}$. Note that first Bressloff in [11] and then Baker and Cowan in [2] use a similar anisotropic function for a continuum model of V1 with long-range horizontal connections without feature space. The second factor of the horizontal connectivity ensures that the long-range connections link cells with similar feature preferences, and is taken to be an even positive, narrowly tuned distribution with $\mathcal{K}(x)=0$ for all $|x|\geq k_c$. In the limit $k_c\to 0$, $\mathcal{K}$ is taken to be the δ-dirac function. The parameter ϵ controls the degree of anisotropy.

2.2. **Symmetries of the model.** The Euclidean group $\mathbf{E}(2)$ is crucial to the analyses in [14, 13] where it acts on $\mathbb{R}^2\times\mathbf{S}^1$ by the so-called "shift-twist" representation due to the anisotropic nature of the lateral connections. In our model, the action of $\mathbf{E}(2)$ on $\mathbb{R}^2\times\mathbf{SPD}(2,\mathbb{R})$ that preserves the structure of the long-range connections in equation (2.4) is given by

$$\begin{aligned}
a\cdot(\mathbf{r},\mathcal{T})&=(\mathbf{r}+a,\mathcal{T})\quad a\in\mathbb{R}^2\\
\mathcal{R}_\theta\cdot(\mathbf{r},\mathcal{T})&=\left(\mathcal{R}_\theta\mathbf{r},\mathcal{R}_\theta\mathcal{T}\mathcal{R}_\theta^{\mathbf{T}}\right)\quad\theta\in\mathbf{S}^1\\
\mathcal{M}_\kappa\cdot(\mathbf{r},\mathcal{T})&=(\mathcal{M}_\kappa\mathbf{r},\mathcal{M}_\kappa\mathcal{T}\mathcal{M}_\kappa^{\mathbf{T}})
\end{aligned} \tag{2.5}$$

where $\mathcal{M}_\kappa$ is the matrix representation of the reflection $(r_1, r_2) \to (r_1, -r_2)$ and $\mathcal{R}_\theta$ is a matrix rotation of angle θ.

The corresponding group action on a function $V : \mathbb{R}^2 \times \mathbf{SPD}(2,\mathbb{R}) \to \mathbb{R}$ is given by:

$$\gamma \cdot V(\mathbf{r}, \mathcal{T}) = V\left(\gamma^{-1} \cdot (\mathbf{r}, \mathcal{T})\right)$$

for all $\gamma \in \mathbf{E}(2)$ and the action on the weight distribution $W(\mathbf{r}, \mathcal{T} \mid \mathbf{r}', \mathcal{T}')$ is

$$\gamma \cdot W(\mathbf{r}, \mathcal{T} \mid \mathbf{r}', \mathcal{T}') = W\left(\gamma^{-1} \cdot (\mathbf{r}, \mathcal{T}) \mid \gamma^{-1} \cdot (\mathbf{r}', \mathcal{T}')\right).$$

It follows that W given by (2.3) and (2.4) is invariant under the action of the Euclidean group defined by equations (2.5). As a consequence, equation (2.1) is equivariant with respect to the symmetry group $\mathbf{E}(2)$ for $h(\mathbf{r}, \mathcal{T}, t) = 0$.

In the limit $\epsilon = 0$, the lateral connectivity function defined in equation (2.4) is called *isotropic* and reduces to

$$W^0_{lat}(\mathbf{r}, \mathcal{T} \mid \mathbf{r}', \mathcal{T}') = \mathcal{J}\left(\|\mathbf{r} - \mathbf{r}'\|\right) \mathcal{K}\left(d\left(\mathcal{T}, \mathcal{T}'\right)\right). \tag{2.6}$$

In that particular case, in addition to Euclidean symmetry, equation (2.1) admits a $\mathbf{GL}(2,\mathbb{R})$-symmetry,. The two actions decouple and are given by:

$$\begin{aligned} \gamma \cdot (\mathbf{r}, \mathcal{T}) &= (\gamma \mathbf{r}, \mathcal{T}) \quad \gamma \in \mathbf{E}(2) \\ M \cdot (\mathbf{r}, \mathcal{T}) &= (\mathbf{r}, M\mathcal{T}M^{\mathbf{T}}) \quad M \in \mathbf{GL}(2,\mathbb{R}). \end{aligned} \tag{2.7}$$

2.3. **The Poincaré disk model.** The feature space $\mathbf{SPD}(2,\mathbb{R})$ of structure tensors is the set of 2×2 symmetric positive definite matrices. This set is a solid open cone in $\mathbb{R}^3$ and a Riemannian manifold with the distance [49]

$$d_{\mathbf{SPD}(2,\mathbb{R})}(\mathcal{T}, \mathcal{T}') = \|\log \mathcal{T}^{-1}\mathcal{T}'\|_F \tag{2.8}$$

where $\|\cdot\|_F$ is the Frobenius norm. Now any $\mathcal{T} \in \mathbf{SPD}(2,\mathbb{R})$ can be written $\mathcal{T} = \delta\tilde{\mathcal{T}}$ with $\delta > 0$ and $\det \tilde{\mathcal{T}} = 1$. Therefore $\mathbf{SPD}(2,\mathbb{R}) = \mathbb{R}^+_* \times \mathbf{SSPD}(2,\mathbb{R})$, the two-dimensional submanifold of symmetric positive definite matrices whose determinant is equal to 1. It can be shown (see appendix A) that the surface $\mathbf{SSPD}(2,\mathbb{R})$ equipped with the Riemannian structure induced by the metric of $\mathbf{SPD}(2,\mathbb{R})$, is isomorphic to the hyperbolic plane which is itself isomorphic to the disk $\mathbb{D} = \{z \in \mathbb{C} \mid |z| < 1\}$ equipped with the hyperbolic distance

$$d_{\mathbb{D}}(z, z') = \operatorname{arctanh} \frac{|z - z'|}{|1 - \bar{z}z'|} \text{ (Poincaré disk).}$$

Therefore, there is an isomorphism between the space of structure tensors and the product space $\mathbb{R}^+_* \times \mathbb{D}$. As shown in [27], the distance in $\mathbf{SPD}(2,\mathbb{R})$ can be written in $(\delta, z) \in \mathbb{R}^+_* \times \mathbb{D}$ coordinates as

$$d_{\mathbf{SPD}(2,\mathbb{R})}(\mathcal{T}, \mathcal{T}') = \sqrt{2 \ln\left(\frac{\delta}{\delta'}\right)^2 + d_{\mathbb{D}}(z, z')^2}.$$

Using the same argument as in [18], we are able to cancel out the dependence on $\delta \in \mathbb{R}^+_*$ which would not play a significant role in the analysis that follows.

Assumption 1. *Equation* (2.1) *is posed on* $\mathbb{R}^2 \times \mathbb{D}$ *from now on.*

The group of isometries of $\mathbb{D}$ is the unitary group $\mathbf{U}(1,1)$, see appendix B for definitions.

One can transcribe the group actions of $\mathbf{E}(2)$ and $\mathbf{U}(1,1)$ defined in equations (2.5) and (2.7) respectively on the space $\mathbb{R}^2 \times \mathbb{D}$. In the anisotropic case we have:

$$\begin{aligned} a \cdot (\mathbf{r}, z) &= (\mathbf{r} + a, z) \quad a \in \mathbb{R}^2 \\ \mathcal{R}_\theta \cdot (\mathbf{r}, z) &= \left(\mathcal{R}_\theta \mathbf{r}, e^{2i\theta} z\right) \quad \theta \in \mathbf{S}^1 \\ \mathcal{M}_\kappa \cdot (\mathbf{r}, z) &= (\kappa \mathbf{r}, \bar{z}). \end{aligned} \tag{2.9}$$

and in the isotropic case ($\epsilon = 0$):

$$\begin{aligned} \gamma \cdot (\mathbf{r}, z) &= (\gamma \mathbf{r}, z) \quad \gamma \in \mathbf{E}(2) \\ g \cdot (\mathbf{r}, z) &= (\mathbf{r}, g \cdot z) \quad g \in \mathbf{U}(1,1) \end{aligned} \tag{2.10}$$

where the action of $g \in \mathbf{U}(1,1)$ on $z \in \mathbb{D}$ is defined in equation (B.1) of appendix B.

If we now write equation (2.1) as an abstract problem of the form:

$$\frac{dV(t)}{dt} = \mathbf{F}(V(t), \mu, \beta, \epsilon) = 0 \tag{2.11}$$

then we can summarize the previous discussion as follows:

1. for all (μ, β, ϵ), $\mathbf{F}(\cdot, \mu, \beta, \epsilon)$ is equivariant with respect to $\mathbf{E}(2)$ with shift-twist action;
2. $\mathbf{F}(\cdot, \mu, \beta, 0)$ is equivariant with respect to $\mathbf{E}(2) \times \mathbf{U}(1,1)$ (isotropic case);
3. $\mathbf{F}(\cdot, \mu, 0, 0)$ is equivariant with respect to $\mathbf{U}(1,1)$ (no lateral connections).

2.4. **Two complementary approaches.** We are interested in the bifurcations from the trivial state $V = 0$ of Equation (2.11) where μ is the bifurcation parameter. Previous works like [25] and [28] have assumed that the pattern arising in the V1 plane was doubly periodic, occurring either on a square or hexagonal lattice. This assumption allows to reduce the bifurcation problem to a finite dimensional center manifold and we shall keep this framework in the present study. We have however an additional complication, of similar type, due to the fact that the feature space of structure tensors, which we assimilate to the Poincaré disc $\mathbb{D}$, is unbounded and has non compact isometry group $\mathbf{U}(1,1)$, which puts a strong obstruction to apply the standard tools of bifurcation theory. To overcome this difficulty we can take two different approaches which we now define.

Problem 1. *Observe that natural images can only produce a bounded set of structure tensors with determinant equal to one. This suggests to restrict ourselves to a bounded domain of the Poincaré disc for the feature space. It is convenient to choose a domain which still preserves the rotational invariance of* (2.9)*. We therefore choose a disc $\Omega \subset \mathbb{D}$ of radius r_ω such that $r_\omega = \tanh(\omega/2) < 1$.*
As suggested by microelectrode recordings, β is small and therefore the lateral connections modulate rather than drive the cortical activity. This suggests to begin to study the case of no lateral coupling: $\beta = 0$ (model of a single hypercolumn defined on Ω) and then use perturbation analysis when anisotropic coupling is switched on: $0 < \beta \ll 1$.

Problem 1 is closely linked to the analysis of [14, 12] for the ring model (the feature space is $\mathbf{S}^1$) and [10, 9] for the spherical model (the feature space is the sphere S^2 which accounts for orientations and spatial frequency), where perturbation theory is used to calculate the eigenvalues and eigenfunctions of the "spatialized" cortical dynamics. Our aim is to use a similar approach in the case of a

bounded domain Ω, with lateral coupling given by equations (2.3) and (2.4). This problem is treated in section 3.

Problem 2. *We consider again the full feature space $\mathbb{D}$ and we rely on the following remark. The anisotropy in lateral connections can be small depending on the animal studied* [46] *and in that case we can assume $\epsilon \approx 0$. This suggests to study first the isotropic case: $\epsilon = 0$, which has symmetry group $\mathbf{E}(2) \times \boldsymbol{U}(1,1)$, for patterns which are periodic both spatially in $\mathbb{R}^2$ and in the feature space $\mathbb{D}$. Then we break the symmetry by switching on $0 < \epsilon \ll 1$, so that it is reduced to $\mathbf{E}(2)$. This forced symmetry breaking is treated as a perturbation of the isotropic case.*

Section 4 is devoted to this problem. This approach was initiated by Golubitsky et al in [28] for the ring model. There is however an important difference: in [28], the symmetry group for one (isolated) hypercolumn is S^1 and it does not take account of the reflections which should naturally occur if the connectivity function W_{loc} did only depend on the distance between angles. In their case the "isotropic" symmetry group is $\mathbf{E}(2) \ltimes S^1$. However if reflections are included in the symmetries, the group becomes the direct product $\mathbf{E}(2) \times \mathbf{O}(2)$. In our case, because we use an explicit expression for W_{loc}, the "isotropic" symmetry group is $\mathbf{E}(2) \times \mathbf{U}(1,1)$.

3. Problem 1: weak anisotropic coupling on a bounded structure tensor space.

3.1. Eigenfunctions of the Laplace-Beltrami operator on Ω.

This section is devoted to the study of the eigenfunctions of the Laplace-Beltrami operator on Ω which will be needed for the spectral analysis of the following parts. We impose Dirichlet conditions on the boundary of the disk. From a physic point of view, this problem is analog to finding the modes of a vibrating membrane in hyperbolic geometry. The Laplace-Beltrami operator $\Delta_{\mathbb{D}}$ on $\mathbb{D}$ in hyperbolic polar coordinates (τ, θ) with $z = \tanh(\tau/2)e^{i\theta}$ is defined by:

$$\Delta_{\mathbb{D}} = \frac{\partial^2}{\partial \tau^2} + \coth(\tau)\frac{\partial}{\partial \tau} + \sinh(\tau)^{-2}\frac{\partial^2}{\partial \theta^2}. \tag{3.1}$$

We are looking for eigensolutions of

$$\begin{cases} -\Delta_{\mathbb{D}} V(z) = \lambda V(z), \quad \forall z \in \Omega, \quad \lambda \in \mathbb{R}^+ \\ \qquad V(z) = 0 \quad \forall z \in \partial\Omega \end{cases} \tag{3.2}$$

which can be written $V_m(z) = e^{im\theta}U_m(\cosh(\tau))$. Replacing the expression of $V_m(z)$ into equation (3.2) and setting $y = \cosh(\tau)$ yields

$$(y^2-1)\ddot{U}_m(y) + 2y\dot{U}_m(y) + \left(\lambda - \frac{m^2}{y^2-1}\right)U_m(y) = 0.$$

We set $-\lambda = l(l+1)$ with $l = -\frac{1}{2} + i\rho$ such that $\lambda = \rho^2 + \frac{1}{4}$. The Legendre functions $\mathcal{P}_l^m$ of the first kind and $\mathcal{Q}_l^m$ of the second kind form a basis of the space of solutions. Solutions $\mathcal{Q}_l^m$ are not physically relevant as they blow up at $\tau = 0$. We write $V_m(z) = e^{im\theta}\mathcal{P}_l^m(\cosh(\tau))$ the other solutions. Finally the solutions of (3.2) which further satisfy $V_m(z) = 0$ for all $z \in \partial\Omega$ can be expressed as $V_m(z) = e^{im\theta}\mathcal{P}_l^m(\cosh(\tau))$ with $\mathcal{P}_l^m(\cosh(\omega)) = 0$. Then for each $m \in \mathbb{Z}$, one

has to impose that $l_{m,n} = -\frac{1}{2} + i\lambda_{m,n}$, where $\lambda_{m,n}$ is the nth root of the function $\lambda \to \mathcal{P}^m_{-\frac{1}{2}+i\lambda}(\cosh(\omega))$. As a consequence, each eigenfunction V can be written:

$$\begin{aligned} V(z) &= \sum_{m\in\mathbb{Z}}\sum_{n\in\mathbb{N}^*} a_{m,n}\mathcal{P}^m_{l_{m,n}}(\cosh(\tau))e^{im\theta} \quad \forall z\in\Omega \text{ and } a_{m,n}\in\mathbb{C} \\ &= \sum_{n=1}^{+\infty} A_{0,n}\mathcal{P}_{l_{m,n}}(\cosh(\tau)) + \sum_{m=1}^{+\infty}\sum_{n=1}^{+\infty} A_{m,n}\mathcal{P}^m_{l_{m,n}}(\cosh(\tau))\cos(m\theta) \\ &\quad + \sum_{m=1}^{+\infty}\sum_{n=1}^{+\infty} B_{m,n}\mathcal{P}^m_{l_{m,n}}(\cosh(\tau))\sin(m\theta) \end{aligned}$$

where $A_{0,n}, A_{m,n}$ and $B_{m,n}$ are real.

From the properties [24]:

$$\mathcal{P}^m_l = \mathcal{P}^m_{-l-1} \text{ and } \mathcal{P}^m_l = \frac{\Gamma(l+m+1)}{\Gamma(l-m+1)}\mathcal{P}^{-m}_l,$$

where Γ is the Gamma function, we can deduce that:

$$\begin{aligned} A_{m,n} &= a_{m,n} + \frac{\Gamma(l_{m,n}-m+1)}{\Gamma(l_{m,n}+m+1)}a_{-m,n} \\ B_{m,n} &= i\left(a_{m,n} - \frac{\Gamma(l_{m,n}-m+1)}{\Gamma(l_{m,n}+m+1)}a_{-m,n}\right). \end{aligned}$$

Proposition 3.1. *For fixed m and ω, the function $\lambda \to \mathcal{P}^m_{-\frac{1}{2}+i\lambda}(\cosh(\omega))$ possesses only isolated simple zeros which satisfy:*

$$0 < \lambda_{m,1} < \lambda_{m,2} < \cdots < \lambda_{m,n} < \ldots \text{ with } \lim_{n\to+\infty}\lambda_{m,n} = +\infty.$$

If we normalize associated Legendre functions such that

$$\mathcal{Y}^m_n(\tau) \overset{def}{=} \mathcal{Y}^m_{l_{m,n}}(\tau) = \frac{\mathcal{P}^m_{-1/2+i\rho_{m,n}}(\cosh\tau)}{p_{m,n}}$$

$$\text{with } p^2_{m,n} \overset{def}{=} \int_0^\omega \left[\mathcal{P}^m_{-1/2+i\rho_{m,n}}(\cosh\tau)\right]^2 \sinh\tau d\tau$$

then

$$< \mathcal{Y}^m_n, \mathcal{Y}^m_{n'} >= \int_0^\omega \mathcal{Y}^m_n(\tau)\mathcal{Y}^m_{n'}(\tau)\sinh\tau d\tau = \delta_{n,n'}.$$

Proof. Multiplying equation (3.2) by $\sinh(\tau)$ we can rewrite the eigenvalue problem as a Sturm-Liouville problem:

$$\frac{d}{d\tau}\left(\sinh(\tau)\frac{dV}{d\tau}(\tau)\right) - \frac{m^2}{\sinh(\tau)}V(\tau) = -\lambda\sinh(\tau)V(\tau), \quad \forall\tau\in]0,\omega] \tag{3.3}$$

with the boundary conditions: $V(\omega) = 0$ and $\lim_{\tau\to0} V(\tau) < +\infty$. We look for eigenvalues of the form $\lambda = \rho^2 + \frac{1}{4}$.

We first assume that $m = 0$ such that equation (3.3) is now defined on $[0,\omega]$ and is a regular Sturm-Liouville problem. Sturm-Liouville theorem for regular problem [70, 16] ensures that the eigenvalues of (3.3) are non-negative, real and simple such that:

$$0 < \lambda_{0,1} < \lambda_{0,2} < \cdots < \lambda_{0,n} < \ldots \text{ with } \lim_{n\to+\infty}\lambda_{0,n} = +\infty.$$

On the other hand, equation (3.3) is a second order differential equation which admits two real linearly independent solutions $\tau \to \mathcal{P}_\nu(\cosh(\tau))$ and $\tau \to \mathcal{Q}_\nu(\cosh(\tau))$

with $\nu = -\frac{1}{2} + i\rho$. As we impose the boundary condition $\lim_{\tau\to 0} V(\tau) < +\infty$, we only keep the solution $\tau \to \mathcal{P}_\nu(\cosh(\tau))$. The other boundary condition imposes that $\mathcal{P}_{-\frac{1}{2}+i\rho}(\cosh(\omega)) = 0$, and if $\rho_{0,n}$ is the nth zero of the analytic function $\rho \to \mathcal{P}_{-\frac{1}{2}+i\rho}(\cosh(\omega))$ we have $\lambda_{0,n} = \rho_{0,n}^2 + \frac{1}{4}$. Finally $(\lambda_{0,n}, \mathcal{P}_{-\frac{1}{2}+i\rho_{0,n}}(\cosh(\cdot))$ is the solution of the eigenvalue problem (3.3). The orthogonality property is a consequence of the simplicity of each eigenvalue and the form of equation (3.3). Take $(\lambda_{0,n}, V_n = \mathcal{P}_{-\frac{1}{2}+i\rho_{0,n}}(\cosh(\cdot))$ and $(\lambda_{0,n'}, V_{n'} = \mathcal{P}_{-\frac{1}{2}+i\rho_{0,n'}}(\cosh(\cdot))$ two solutions of equation (3.3) then:

$$\begin{aligned}\int_0^\omega V_n(\tau)V_{n'}(\tau)\sinh(\tau)d\tau &= -\frac{1}{\lambda_{0,n}}\int_0^\omega \frac{d}{d\tau}\left(\sinh(\tau)\frac{dV_n}{d\tau}(\tau)\right)V_{n'}(\tau)d\tau \\ &= \frac{1}{\lambda_{0,n}}\int_0^\omega \sinh(\tau)\frac{dV_n}{d\tau}(\tau)\frac{dV_{n'}}{d\tau}(\tau)d\tau \\ &= \frac{\lambda_{0,n'}}{\lambda_{0,n}}\int_0^\omega V_n(\tau)V_{n'}(\tau)\sinh(\tau)d\tau.\end{aligned}$$

This implies that for $n \neq n'$, $\int_0^\omega V_n(\tau)V_{n'}(\tau)\sinh(\tau)d\tau = 0$.

Next, suppose $m \geq 1$. The eigenvalue problem (3.3) is now a singular Sturm-Liouville problem because of the singularity at $\tau = 0$. Nevertheless, it is still possible to prove the existence of real non-negative and simple eigenvalues of (3.3) ([70, 16]):

$$0 < \lambda_{m,1} < \lambda_{m,2} < \cdots < \lambda_{m,n} < \dots \text{ with } \lim_{n\to+\infty}\lambda_{m,n} = +\infty.$$

It is straightforward to see that $(\lambda_{m,n}, \mathcal{P}^m_{-\frac{1}{2}+i\rho_{m,n}}(\cosh(\cdot))$ is a solution of the eigenvalue problem. The proof of the orthogonality property follows the same lines as for the case $m = 0$, with the additional remark that for all $m \geq 1$ the function

$$\tau \to \sinh(\tau)^{-1}\mathcal{P}^m_{-\frac{1}{2}+i\rho_{m,n}}(\cosh(\tau))\mathcal{P}^m_{-\frac{1}{2}+i\rho_{m,n'}}(\cosh(\tau))$$

is integrable on $]0, \omega]$ for all $n, n' \in \mathbb{N}^*$. □

The multiplicity of the eigenvalues of the Laplace-Beltrami operator is a complex problem. As for the zeros of Bessel functions [66], between two consecutive zeros of $\lambda \to \mathcal{P}^m_{-\frac{1}{2}+i\lambda}(\cosh(\omega))$ there exists one zero of $\lambda \to \mathcal{P}^{m+1}_{-\frac{1}{2}+i\lambda}(\cosh(\omega))$ [43]. This implies that the multiplicity of $\lambda_{0,1}$ is one and the multiplicity of $\lambda_{1,1}$ is two. We further have $0 < \lambda_{0,1} < \lambda_{1,1} < \cdots$.

3.2. **Study of an isolated hypercolumn.**

3.2.1. *Linear stability analysis.* We rewrite equation (2.1) for $\beta = 0$ in the lateral coupling function in (τ, θ)-coordinates.

$$\begin{aligned}\frac{\partial V(\mathbf{r},\tau,\theta,t)}{\partial t} = -V(\mathbf{r},\tau,\theta,t) + \int_0^\omega\int_0^{2\pi} W_{loc}\left(d_{\mathbb{D}}\left(\tanh(\tau/2)e^{i\theta}, \tanh(\tau'/2)e^{i\theta'}\right)\right) \\ \times S(\mu V(\mathbf{r},\tau',\theta',t))\sinh(\tau')d\tau'd\theta'\end{aligned} \tag{3.4}$$

The local connectivity function can be expressed in a compact form as

$$\begin{aligned}W_{loc}(\tau,\tau' \mid \theta-\theta') &\stackrel{def}{=} W_{loc}\left(d_{\mathbb{D}}\left(\tanh(\tau/2)e^{i\theta}, \tanh(\tau'/2)e^{i\theta'}\right)\right) \\ &= \sum_{m=0}^{+\infty}\sum_{n\in\mathbb{N}^*}\widehat{W}_{m,n}\mathcal{Y}^m_n(\tau)\mathcal{Y}^m_n(\tau')\cos(m(\theta-\theta')).\end{aligned} \tag{3.5}$$

Equation (3.4) presents an $\mathbf{O}(2)$ symmetry with action:

$$\begin{aligned}\varphi \cdot (\tau, \theta) &= (\tau, \theta + \varphi) \quad \varphi \in [0, 2\pi] \\ s \cdot (\tau, \theta) &= (\tau, -\theta).\end{aligned}$$

With the fact that $S(0) = 0$ in the definition of the sigmoidal function S, the fully symmetric state $V = 0$ is always a solution of (3.4) for all values of the parameter μ and its uniqueness has been discussed in [27]. To study the linear stability of the trivial state $V = 0$, we have to look at solutions of the linearized equation

$$\begin{aligned}\frac{\partial V(\mathbf{r}, \tau, \theta, t)}{\partial t} = -V(\mathbf{r}, \tau, \theta, t) + \mu s_1 \int_0^\omega \int_0^{2\pi} W_{loc}\left(\tau, \tau' \mid \theta - \theta'\right) \\ \times V(\mathbf{r}, \tau', \theta', t) \sinh(\tau') d\tau' d\theta'.\end{aligned} \tag{3.6}$$

with $s_1 = S'(0)$, of the form $e^{\sigma t} U(\mathbf{r}, \tau, \theta)$. Substituting the distribution (3.5) for W_{loc} and using orthogonality relation shows that the dispersion relation is given by:

$$\sigma_{n,m} = -1 + \mu s_1 \widehat{W}_{m,n}$$

with corresponding eigenvectors $\mathcal{Y}_n^m(\tau)\cos(m\theta)$ and $\mathcal{Y}_n^m(\tau)\sin(m\theta)$ if $m \geq 1$, $\mathcal{Y}_n^0(\tau)$ if $m = 0$. Thus the eigenvalue $\sigma_{n,m}$ is at least 2-fold degenerate for $m \geq 1$. If we denote

$$\widehat{W}_{M,N} = \max\{\widehat{W}_{m,n} \mid (m, n) \in \mathbb{N} \times \mathbb{N}^*\}$$

then $V = 0$ becomes unstable at a critical value $\mu_c = \left(s_1 \widehat{W}_{M,N}\right)^{-1}$.

The cases $(M = 0, N = 1)$ and $(M = 1, N = 1)$ are relevant from a biological point of view. If $M = 0$ and $N = 1$, sufficiently close to the bifurcation point, the resulting activity profile satisfies

$$V(\mathbf{r}, \tau, \theta) = a(\mathbf{r}) \mathcal{Y}_1(\tau)$$

and if $M = 1$ and $N = 1$ we have:

$$V(\mathbf{r}, \tau, \theta) \quad = \quad \alpha(\mathbf{r}) \mathcal{Y}_1^1(\tau) \cos\left(\theta - \phi(\mathbf{r})\right).$$

In the first case, the new steady state shows no orientation preference as it can be seen in figure 3(a) where the region of high activity is centered at $z = 0$. In the second case, the response is both unimodal with respect to τ and θ, see figure 3(b). The occurrence of a tuned surface peaked at some angle $\phi(\mathbf{r})$ corresponds to the presence of local contour there. The angle $\phi(\mathbf{r})$ for each tuning surface is arbitrary which reflects the $\mathbf{O}(2)$ equivariance of equation (3.4). Without any lateral connections, the overall tuned response is uncorrelated across the cortex. As explained in [14], the presence of anisotropy has for consequence to correlate the peaks of the tuning surfaces at different locations.

3.2.2. *Pitchfork bifurcation with* $\mathbf{O}(2)$ *symmetry.* We have a Pitchfork bifurcation with $\mathbf{O}(2)$ symmetry at the critical point $\mu = \mu_c$. In order to be able to compare our results with those obtained in the Ring Model of orientation, we select unimodal solution in the θ variable: $M = 1$ and the τ variable $N = 1$. Close to the bifurcation point $(V = 0, \mu = \mu_c)$ there exists a polynomial change of variables of the form

$$V(\mathbf{r}, \tau, \theta, t) = A(\mathbf{r}, t)\zeta_1(\tau, \theta) + B(\mathbf{r}, t)\zeta_2(\tau, \theta) + \Psi(A(\mathbf{r}, t), B(\mathbf{r}, t), \mu - \mu_c)$$

with

$$\zeta_1(\tau, \theta) = \mathcal{Y}_1^1(\tau)\cos(\theta) \text{ and } \zeta_2(\tau, \theta) = \mathcal{Y}_1^1(\tau)\sin(\theta)$$

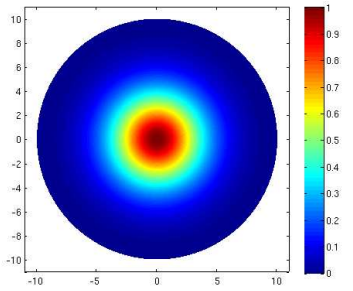

(a) Mode $(0,1)$ with $\lambda_{0,1} = 0.2798$.

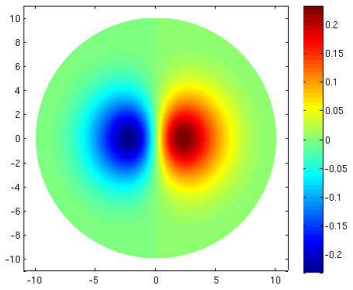

(b) Mode $(1,1)$ with $\lambda_{1,1} = 0.334$.

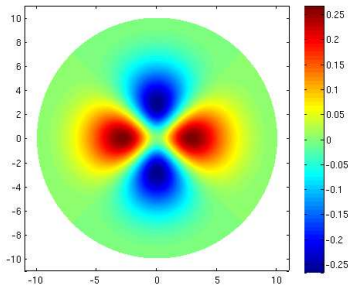

(c) Mode $(2,1)$ with $\lambda_{2,1} = 0.3585$.

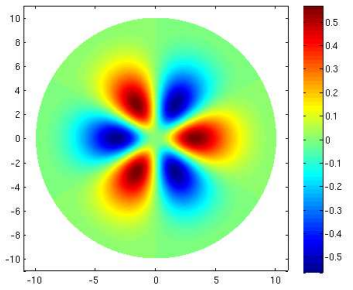

(d) Mode $(3,1)$ with $\lambda_{3,1} = 0.3753$.

FIGURE 3. Plot of solution of the form $\mathcal{P}^m_{l_{m,n}}(\cosh(\tau))\cos(m\theta)$ with $(\tau,\theta) \in [0,\omega] \times [0,2\pi]$ and $l_{m,n} = -\frac{1}{2} + i\lambda_{m,n}$.

which transforms equation (3.4) into the normal form

$$\begin{aligned} \frac{dA}{dt} &= \left[\frac{\mu - \mu_c}{\mu_c} + \varpi(A^2 + B^2)\right] A + \text{h.o.t.} \\ \frac{dB}{dt} &= \left[\frac{\mu - \mu_c}{\mu_c} + \varpi(A^2 + B^2)\right] B + \text{h.o.t.} \end{aligned} \tag{3.7}$$

and ϖ can be expressed as

$$\varpi = \frac{\mu_c^3 \pi \widehat{W}_{1,1}}{4}\left(\frac{s_3\Lambda}{2} + \mu_c s_2^2 \sum_{n\in\mathbb{N}^*}\left[\frac{\pi\widehat{W}_{0,n}\left(\gamma_{0,n}\right)^2}{\left(1 - \mu_c s_1 2\pi\widehat{W}_{0,n}\right)} + \frac{\pi\widehat{W}_{2,n}\left(\gamma_{2,n}\right)^2}{4\left(1 - \mu_c s_1 \pi\widehat{W}_{2,n}\right)}\right]\right) \tag{3.8}$$

with $s_2 = S''(0), s_3 = S'''(0)$ and

$$\begin{aligned} \Lambda &= \int_0^\omega \left(\mathcal{Y}_1^1(\tau)\right)^4 \sinh(\tau) d\tau \\ \gamma_{k,n} &= \int_0^\omega \mathcal{Y}_n^k(\tau') \left(\mathcal{Y}_1^1(\tau')\right)^2 \sinh(\tau') d\tau'. \end{aligned}$$

Proof. These formulas are derived in appendix C. □

The sign of ϖ determines if the bifurcation is subcritical or supercritical. If $\varpi < 0$, the Pitchfork is oriented towards the increasing μs (supercritical) otherwise it points towards the decreasing μs (subcritical). In this latter case, it can be shown [64] that the bifurcated branch has to turn around which produces two additional solutions on each branch. As it has been noticed in [65] in the case of the ring model of orientation, $\varpi > 0$ does not give a biological plausible behaviour of the network. This is why we impose the condition $\varpi < 0$, which gives a constrain on the threshold T of the sigmoidal function defined in equation (2.2) and the coefficients $\widehat{W}_{m,n}$ of the coupling function W_{loc}. In the simplified case where $\widehat{W}_{0,1} = -1$ and $\widehat{W}_{m,n} = 0$ for all $(m,n) \in \mathbb{N} \times \mathbb{N}^* \setminus \{(0,1),(1,1)\}$, we plot in figure 4 the sign of ϖ as a function of T and $\widehat{W}_{1,1}$.

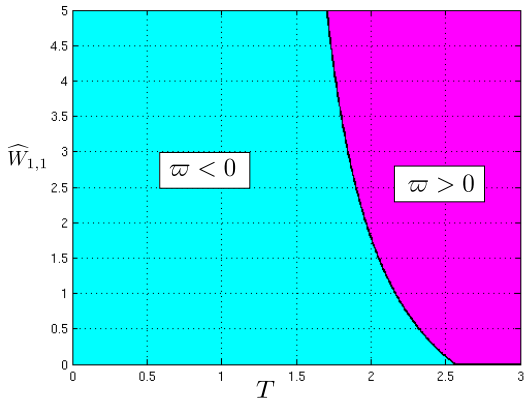

FIGURE 4. Plot of the sign of ϖ as a function of T and $\widehat{W}_{1,1}$.

3.3. **Weak lateral interactions.** We now turn on the lateral interactions: $\beta \neq 0$. We have already mentioned in Problem 1 that the lateral connections modulate rather than drive the cortical activity. This is why we will work in the regime where $0 < \beta \ll 1$. In order to be able to present some analytic results, we select a simplified version of the function $\mathcal{K}$ (this is the limit case $k_c \to 0$ in the definition of $\mathcal{K}$ in equation (2.4)):

$$\mathcal{K}(\tau,\theta \mid \tau',\theta') = \frac{1}{\sinh(\tau)}\delta_{\tau,\tau'}\delta_{\theta,\theta'}.$$

3.3.1. *Eigenvalues and eigenfunctions of the linear problem.* We first linearize equation (2.1) close to the fully symmetric state $V(\mathbf{r},\tau,\theta,t) = 0$.

$$\frac{\partial V(\mathbf{r},\tau,\theta,t)}{\partial t} = -V(\mathbf{r},\tau,\theta,t) + \mu s_1 \left[\int_0^\omega \int_0^{2\pi} W_{loc}\left(\tau,\tau' \mid \theta-\theta'\right) \times V(\mathbf{r},\tau',\theta',t)\sinh(\tau')d\tau' d\theta' + \beta \int_{\mathbb{R}^2} \mathcal{J}(\mathbf{r}-\mathbf{r}',\tau,\theta)V(\mathbf{r}',\tau,\theta)d\mathbf{r}'\right], \tag{3.9}$$

where we have set:

$$\mathcal{J}(\mathbf{r}-\mathbf{r}',\tau,\theta) \stackrel{def}{=} \mathcal{J}\left(\sqrt{(\mathbf{r}-\mathbf{r}')^{\mathbf{T}}(\mathbf{I}_2+\epsilon\mathcal{T}(\tau,\theta))(\mathbf{r}-\mathbf{r}')}\right)$$

with $\mathcal{T}(\tau,\theta)$ given through the "$\mathbb{D}$ to $\mathbf{SSPD}(2,\mathbb{R})$" dictionary in appendix A by

$$\mathcal{T}(\tau,\theta) = \begin{pmatrix} a(\tau,\theta) & c(\tau,\theta) \\ c(\tau,\theta) & b(\tau,\theta) \end{pmatrix}$$

and

$$\begin{aligned} a(\tau,\theta) &= \frac{1+\tanh(\tau/2)^2+2\tanh(\tau/2)\cos(\theta)}{1-\tanh(\tau/2)^2} \\ b(\tau,\theta) &= \frac{1+\tanh(\tau/2)^2-2\tanh(\tau/2)\cos(\theta)}{1-\tanh(\tau/2)^2} \\ c(\tau,\theta) &= \frac{2\tanh(\tau/2)\sin(\theta)}{1-\tanh(\tau/2)^2}. \end{aligned}$$

We look for perturbations of the form $e^{\sigma t}u_{\mathbf{k}}(\tau,\theta)e^{i\mathbf{k}\cdot\mathbf{r}}+$ cc with $\mathbf{k}=q(\cos\varphi,\sin\varphi)$ and $u_{\mathbf{k}}(\tau,\theta) = u(\tau,\theta-2\varphi)$. Equation (3.9) leads to the eigenvalue problem for $(\sigma,u(\tau,\theta))$:

$$\begin{aligned} \sigma u(\tau,\theta) = &-u(\tau,\theta)+\mu s_1\beta\widetilde{\mathcal{J}}_{\mathbf{k}}(\tau,\theta+2\varphi)u(\tau,\theta) \\ &+\mu s_1\int_0^{\omega}\int_0^{2\pi} W_{loc}\left(\tau,\tau' \mid \theta-\theta'\right)u(\tau',\theta')\sinh(\tau')d\tau' d\theta' \end{aligned} \tag{3.10}$$

with

$$\widetilde{\mathcal{J}}_{\mathbf{k}}(\tau,\theta+2\varphi) = \int_{\mathbb{R}^2}\mathcal{J}(\mathbf{r}-\mathbf{r}',\tau,\theta+2\varphi)e^{i\mathbf{k}\cdot(\mathbf{r}-\mathbf{r}')}d\mathbf{r}'.$$

Due to the rotational invariance of the lateral coupling (2.4) with shift-twist action, the function $\widetilde{\mathcal{J}}_{\mathbf{k}}(\tau,\theta+2\varphi)$ only depends upon q the magnitude of vector $\mathbf{k}\in\mathbb{R}^2$. This is why $(\sigma,u(\tau,\theta))$ given by equation (3.10) also only depends upon q. Expanding $u(\tau,\theta)$ on the basis $\left(\mathcal{Y}_n^m(\tau)\cos(m\theta),\mathcal{Y}_n^m(\tau)\sin(m\theta)\right)_{m\in\mathbb{Z},n\geq 1}$ we obtain:

$$u(\tau,\theta) = \sum_{n=1}^{+\infty}A_{0,n}(q)\mathcal{Y}_n(\tau)+\sum_{m=1}^{+\infty}\sum_{n=1}^{+\infty}\mathcal{Y}_n^m(\tau)\left(A_{m,n}(q)\cos(m\theta)+B_{m,n}(q)\sin(m\theta)\right).$$

Taking the scalar product of equation (3.10) with $\mathcal{Y}_n, \mathcal{Y}_n^m\cos(m\theta)$ and $\mathcal{Y}_n^m\sin(m\theta')$ gives respectively:

$$\begin{aligned} \left[\frac{\sigma+1}{\mu s_1}-\widehat{W}_{0,n}\right]A_{0,n}(q) &= \beta\sum_{m'\in\mathbb{N}}\sum_{n'\in\mathbb{N}^*}\widetilde{\mathcal{J}}^0_{0n,m'n'}(q)A_{m',n'}(q) \\ \left[\frac{\sigma+1}{\mu s_1}-\widehat{W}_{m,n}\right]A_{m,n}(q) &= \beta\sum_{m'\in\mathbb{N}}\sum_{n'\in\mathbb{N}^*}\widetilde{\mathcal{J}}^+_{mn,m'n'}(q)A_{m',n'}(q) \\ \left[\frac{\sigma+1}{\mu s_1}-\widehat{W}_{m,n}\right]B_{m,n}(q) &= \beta\sum_{m'\in\mathbb{N}^*}\sum_{n'\in\mathbb{N}^*}\widetilde{\mathcal{J}}^-_{mn,m'n'}(q)B_{m',n'}(q) \end{aligned}$$

where

$$\widetilde{\mathcal{J}}^0_{0n,m'n'}(q) = \frac{1}{2\pi}\int_0^\omega\int_0^{2\pi} \widetilde{\mathcal{J}}_{\mathbf{k}}(\tau,\theta+2\varphi)\mathcal{Y}_n(\tau)\mathcal{Y}^{m'}_{n'}(\tau)\cos(m'\theta)\sinh(\tau)d\tau d\theta$$
$$\widetilde{\mathcal{J}}^+_{mn,m'n'}(q) = \frac{1}{\pi}\int_0^\omega\int_0^{2\pi} \widetilde{\mathcal{J}}_{\mathbf{k}}(\tau,\theta+2\varphi)\mathcal{Y}^m_n(\tau)\mathcal{Y}^{m'}_{n'}(\tau)\cos(m\theta)\cos(m'\theta)\sinh(\tau)d\tau d\theta$$
$$\widetilde{\mathcal{J}}^-_{mn,m'n'}(q) = \frac{1}{\pi}\int_0^\omega\int_0^{2\pi} \widetilde{\mathcal{J}}_{\mathbf{k}}(\tau,\theta+2\varphi)\mathcal{Y}^m_n(\tau)\mathcal{Y}^{m'}_{n'}(\tau)\sin(m\theta)\sin(m'\theta)\sinh(\tau)d\tau d\theta.$$

Based on the analysis made for $\beta = 0$, we assume that

$$\widehat{W}_{1,1} = \max\{\widehat{W}_{m,n} \mid (m,n) \in \mathbb{N}\times\mathbb{N}^*\}.$$

There is a $\mathbf{k}$-dependent splitting of the degenerate eigenvalue σ associated to the mode $(1,1)$ and denoting the characteristic size of such a splitting by $\delta\sigma = \mathcal{O}(\beta)$, we impose the condition that $\delta\sigma \ll \mu\Delta\widehat{W}$, where $\Delta\widehat{W} = \min\{\widehat{W}_{1,1} - \widehat{W}_{m,n}, m \neq 1 \text{ and } n \neq 1\}$. We can introduce the following perturbation expansions and solve the resulting hierarchy of equations to successive orders in β:

$$\frac{\sigma_\pm + 1}{\mu} = \widehat{W}_{1,1} + \beta\sigma^{(1)}_\pm + \beta^2\sigma^{(2)}_\pm + \dots$$
$$A_{m,n}(q) = A(q)\delta_{m,1}\delta_{n,1} + \beta A^{(1)}_{m,n}(q) + \beta^2 A^{(2)}_{m,n}(q) + \dots$$
$$B_{m,n}(q) = B(q)\delta_{m,1}\delta_{n,1} + \beta B^{(1)}_{m,n}(q) + \beta^2 B^{(2)}_{m,n}(q) + \dots$$

Setting $m = 1$ and $n = 1$ we can collect the $\mathcal{O}(\beta)$ terms and get:

$$\sigma^{(1)}_\pm = \widetilde{\mathcal{J}}^\pm_{11,11}(q)$$
$$A^{(1)}_{m,n}(q) = \frac{\widetilde{\mathcal{J}}^+_{mn,11}(q)A(q)}{\widehat{W}_{1,1} - \widehat{W}_{m,n}}$$
$$B^{(1)}_{m,n}(q) = \frac{\widetilde{\mathcal{J}}^-_{mn,11}(q)B(q)}{\widehat{W}_{1,1} - \widehat{W}_{m,n}}.$$

For the $\mathcal{O}(\beta^2)$ terms we obtain two equations:

$$\left[\sigma^{(1)}_+ - \widetilde{\mathcal{J}}^+_{11,11}(q)\right] A^{(1)}_{1,1}(q) + \sigma^{(2)}_+ A(q) = \sum_{(m',n')\neq(1,1)} \widetilde{\mathcal{J}}^+_{11,m'n'}(q)A^{(1)}_{m',n'}(q)$$
$$\left[\sigma^{(1)}_- - \widetilde{\mathcal{J}}^-_{11,11}(q)\right] B^{(1)}_{1,1}(q) + \sigma^{(2)}_- B(q) = \sum_{(m',n')\neq(1,1)} \widetilde{\mathcal{J}}^-_{11,m'n'}(q)B^{(1)}_{m',n'}(q)$$

which give:

$$\Rightarrow \lambda^{(2)}_\pm = \sum_{(m',n')\neq(1,1)} \frac{\left(\widetilde{\mathcal{J}}^\pm_{11,m'n'}(q)\right)^2}{\widehat{W}_{1,1} - \widehat{W}_{m',n'}}.$$

Finally we have the following proposition.

Proposition 3.2. *The two dispersion relations are given by:*

$$\sigma_{\pm} = -1 + \mu s_1 \left[\widehat{W}_{1,1} + \beta \widetilde{\mathcal{J}}^{\pm}_{11,11}(q) + \beta^2 \sum_{(m',n') \neq (1,1)} \frac{\left(\widetilde{\mathcal{J}}^{\pm}_{11,m'n'}(q) \right)^2}{\widehat{W}_{1,1} - \widehat{W}_{m',n'}} + \mathcal{O}(\beta^2) \right] \tag{3.11}$$

and $u_{\mathbf{k}}(\tau,\theta) = u^{\pm}_{\mathbf{k}}(\tau,\theta)$ *where to* $\mathcal{O}(\beta)$*:*

$$u^{+}_{\mathbf{k}}(\tau,\theta) = \mathcal{Y}^1_1(\tau)\cos(\theta - 2\varphi) + \beta \sum_{(m,n)\neq(1,1)} \mathcal{Y}^m_n(\tau) \frac{\widetilde{\mathcal{J}}^{+}_{mn,11}(q)}{\widehat{W}_{1,1} - \widehat{W}_{m,n}} \cos(m(\theta - 2\varphi)) \tag{3.12}$$

$$u^{-}_{\mathbf{k}}(\tau,\theta) = \mathcal{Y}^1_1(\tau)\sin(\theta - 2\varphi) + \beta \sum_{(m,n)\neq(1,1)} \mathcal{Y}^m_n(\tau) \frac{\widetilde{\mathcal{J}}^{-}_{mn,11}(q)}{\widehat{W}_{1,1} - \widehat{W}_{m,n}} \sin(m(\theta - 2\varphi)). \tag{3.13}$$

3.3.2. *Discussion.* If we suppose that $\mathcal{H}_{\pm}(q) = \widehat{W}_{1,1} + \beta \widetilde{\mathcal{J}}^{\pm}_{11,11}(q)$ has a unique maximum at $q = q_{\pm} \neq 0$. We define $q_c = q_+$ if $\mathcal{H}_+(q_+) > \mathcal{H}_-(q_-)$ and $q_c = q_-$ if $\mathcal{H}_+(q_+) < \mathcal{H}_-(q_-)$, then the homogeneous state $a(\mathbf{r},\tau,\theta) = 0$ is marginally stable at $\mu_c = (s_1\mathcal{H}_+(q_c))^{-1}$ if $q_c = q_+$ and at $\mu_c = (s_1\mathcal{H}_-(q_c))^{-1}$ if $q_c = q_-$. From the rotation invariance, all modes lying on the critical circle $\|\mathbf{k}\| = q_c$ become neutrally stable at $\mu = \mu_c$. The question of the occurrence of even or odd patterns depends of the specific form of the lateral connection $\mathcal{J}$ in equation (2.4).

The infinite degeneracy of the modes on the critical circle can be reduced to a finite set of modes by restricting solutions to be doubly periodic functions on the Euclidean plane, for which we recall some basic properties. Let ℓ_1, ℓ_2 be a basis of $\mathbb{R}^2$. The set $\mathcal{L} = \{2\pi m_1\ell_1 + 2\pi m_2\ell_2 \mid (m_1,m_2) \in \mathbb{Z}^2\}$ is a discrete subgroup of $\mathbb{R}^2$, called a planar lattice. If we denote by H the largest subgroup of $\mathbf{O}(2)$ which preserves the lattice, then the symmetry group $\Gamma_{\mathcal{L}}$ of the lattice is generated by the semi-direct product $\Gamma_{\mathcal{L}} = H \ltimes \mathbb{T}^2$, where $\mathbb{T}^2$ is the 2-torus. The group H is called the holohedry of the lattice. We also define the dual lattice of $\mathcal{L}$ by $\mathcal{L}^* = \{2\pi m_1\mathbf{k}_1 + 2\pi m_2\mathbf{k}_2 \mid (m_1,m_2) \in \mathbb{Z}^2\}$ with $\ell_i \cdot \mathbf{k}_j = \delta_{i,j}$. A function $a : \mathbb{R}^2 \times \Omega \to \mathbb{R}$ is doubly periodic with respect to $\mathcal{L}$ if $a(\mathbf{r}+\ell,\tau,\theta) = a(\mathbf{r},\tau,\theta)$ for every $\ell \in \mathcal{L}$. We summarize in table 1 the different holohedries of the hexagonal, square and rhombic lattice.

Name	Holohedry	ℓ_1	ℓ_2	$\mathbf{k}_1$	$\mathbf{k}_2$
Hexagonal	$\mathbf{D}_6$	$(1, \frac{1}{\sqrt{3}})$	$(0, \frac{2}{\sqrt{3}})$	$(1,0)$	$(-\frac{1}{2}, \frac{\sqrt{3}}{2})$
Square	$\mathbf{D}_4$	$(1,0)$	$(0,1)$	$(1,0)$	$(0,1)$
Rhombic	$\mathbf{D}_2$	$(1, -\cot\theta)$	$(0, \cot\theta)$	$(1,0)$	$(\cos\theta, \sin\theta)$

TABLE 1. Lattices in two dimension with their holohedry. $0 < \theta < \frac{\pi}{2}$, $\theta \neq \frac{\pi}{3}$.

The action of $\Gamma_{\mathcal{L}}$ on the space of doubly periodic functions is the one induced from the action of $\mathbf{E}(2)$ on $\mathbb{R}^2 \times \Omega$ given in (2.9). We consider only bifurcations

based on dual wave vectors of shortest (unit) length and assume that the critical eigenspace $V_{\mathbf{k}}$ consists of functions of the form:

$$a(\mathbf{r},\tau,\theta)=\sum_{j=1}^{s} z_j u_{\mathbf{k}_j}(\tau,\theta)e^{i\mathbf{k}_j\cdot\mathbf{r}}+\text{c.c.} \tag{3.14}$$

where $(z_1,\dots,z_s)\in\mathbb{C}^s$ with $s=2$ for square or rhombic lattices and $s=3$ for hexagonal lattices. It was shown in [13] that the subspace $V_{\mathbf{k}}$ decomposes into two nonisomorphic absolutely irreducible representations of $\Gamma_{\mathcal{L}}$: $V_{\mathbf{k}}=V_{\mathbf{k}}^+\oplus V_{\mathbf{k}}^-$, where $V_{\mathbf{k}}^+$ is the space of even eigenfunctions and $V_{\mathbf{k}}^-$ is the space of odd eigenfunctions in θ. The actions of the group $\Gamma_{\mathcal{L}}$ on $V_{\mathbf{k}}^+$ and $V_{\mathbf{k}}^-$ can be explicitly written down for both the square or rhombic and hexagonal lattices and are given in [14].

Finally, by applying the Equivariant Branching Lemma [29, 19], we can show the existence of branches of solution for each of the axial subgroups of $\Gamma_{\mathcal{L}}$. A subgroup $H\subset\Gamma_{\mathcal{L}}$ is axial if the dimension of the space of vectors that are fixed by H is equal to unity. All these axial subgroups have been calculated in [13, 14] and lead to even and odd planforms. In particular, the perturbation analysis made in the previous part shows that $u_{\mathbf{k}}(\tau,\theta)$ in equation (3.14) can take the forms:

(i) $u_{\mathbf{k}}(\tau,\theta)\approx\mathcal{Y}_1^1(\tau)\cos(\theta-2\varphi)$ for even planforms (equation (3.12)),
(ii) $u_{\mathbf{k}}(\tau,\theta)\approx\mathcal{Y}_1^1(\tau)\sin(\theta-2\varphi)$ for odd planforms (equation (3.13)).

The reduced feature space model for structure tensors is then a direct generalization of the model developed by Bressloff et al in [13, 14] but it does not predict new planforms.

4. Problem 2: bifurcation of doubly periodic planforms in both $\mathbb{R}^2$ and $\mathbb{D}$.

In this section, we adopt the strategy developed in [28]. We will determine solutions to symmetry-breaking bifurcations in the isotropic case ($\epsilon=0$), with symmetry group $\mathbf{E}(2)\times\mathbf{U}(1,1)$, and then study how these solutions change when anisotropy is introduced as a forced symmetry-breaking parameter ($0<\epsilon\ll 1$).

4.1. Bifurcation problem.

First of all we rewrite equation (2.5) on $\mathbb{R}^2\times\mathbb{D}$ with W_{lat}^0 in the definition of (2.3), which gives

$$\begin{aligned}\frac{\partial V(\mathbf{r},z,t)}{\partial t}=&-V(\mathbf{r},z,t)+\int_{\mathbb{D}} W_{loc}\left(d_{\mathbb{D}}(z,z')\right)S(\mu V(\mathbf{r},z',t))\mathrm{dm}(z')\\&+\beta\int_{\mathbb{D}}\int_{\mathbb{R}^2}\mathcal{J}(\|\mathbf{r}-\mathbf{r}'\|)\mathcal{K}\left(d_{\mathbb{D}}(z,z')\right)S(\mu V(\mathbf{r}',z',t))\mathrm{dm}(z')d\mathbf{r}'.\end{aligned} \tag{4.1}$$

With the fact that $S(0)=0$ in the definition of the sigmoidal function S, the fully symmetric state $V=0$ is always a solution of (4.1) for all values of the parameter μ and its uniqueness has been discussed in [27]. To study the linear stability of the trivial state $V=0$, we have to look at solutions of the linearized equation

$$\begin{aligned}\frac{\partial V(\mathbf{r},z,t)}{\partial t}=&-V(\mathbf{r},z,t)+\mu s_1\int_{\mathbb{D}} W_{loc}\left(d_{\mathbb{D}}(z,z')\right)V(\mathbf{r},z',t)\mathrm{dm}(z')\\&+\beta\mu s_1\int_{\mathbb{D}}\int_{\mathbb{R}^2}\mathcal{J}(\|\mathbf{r}-\mathbf{r}'\|)\mathcal{K}\left(d_{\mathbb{D}}(z,z')\right)V(\mathbf{r}',z',t)\mathrm{dm}(z')d\mathbf{r}'.\end{aligned} \tag{4.2}$$

with $s_1 = S'(0)$ of the form $e^{\sigma t}U(\mathbf{r}, z)$. Solutions must satisfy the eigenvalue problem:

$$\begin{aligned}(\sigma+1)U(\mathbf{r},z) = \mu s_1 \int_{\mathbb{D}} W_{loc}\left(d_{\mathbb{D}}(z,z')\right) U(\mathbf{r},z')\mathrm{dm}(z') \\ + \beta\mu s_1 \int_{\mathbb{D}}\int_{\mathbb{R}^2} \mathcal{J}(\|\mathbf{r}-\mathbf{r}'\|)\mathcal{K}\left(d_{\mathbb{D}}(z,z')\right) U(\mathbf{r}',z')\mathrm{dm}(z')d\mathbf{r}'.\end{aligned} \tag{4.3}$$

Because of the $\mathbf{E}(2)\times\mathbf{U}(1,1)$ equivariance of equation (4.1), solutions of (4.3) are plane waves in $\mathbb{R}^2\times\mathbb{D}$. Let b be a point on the circle $\partial\mathbb{D}$, which we may take equal to $b_1 = 1$ after a suitable rotation. For $z\in\mathbb{D}$, we define the "inner product" $\langle z, b\rangle$ as the algebraic distance to the origin of the (unique) horocycle based at b and passing through z. This distance is defined as the hyperbolic signed length of the segment $O\xi$ where ξ is the intersection point of the horocycle and the line (geodesic) Ob. Note that $\langle z, b\rangle$ does not depend on the position of z on the horocycle. In other words, $\langle z, b\rangle$ is invariant under the action of the one-parameter group N (see definition in appendix B). The "hyperbolic plane waves"

$$e_{\rho,b}(z) = e^{(i\rho+\frac{1}{2})\langle z,b\rangle},\ \rho\in\mathbb{C},$$

satisfy

$$-\Delta_{\mathbb{D}}\, e_{\rho,b} = (\rho^2+\frac{1}{4})e_{\rho,b},$$

where $\Delta_{\mathbb{D}}$ is defined for $z = z_1 + iz_2\in\mathbb{D}$ by

$$\Delta_{\mathbb{D}} = \frac{(1-z_1^2-z_2^2)^2}{4}\left(\frac{\partial^2}{\partial z_1^2}+\frac{\partial^2}{\partial z_2^2}\right). \tag{4.4}$$

Real eigenvalues $-(\rho^2+\frac{1}{4})$ of $\Delta_{\mathbb{D}}$ correspond to taking ρ real or $\rho\in i\mathbb{R}$. The latter case is irrelevant for our study as it corresponds to exponentially diverging eigenfunctions. Therefore the real spectrum of $\triangle$ is continuous and is bounded from above by $-1/4$. Functions $e_{\rho,b}$ are the elementary eigenfunctions with which Helgason [32] built a Fourier transform theory for the Poincaré disc, see [32].

Definition 4.1. Given a function f on $\mathbb{D}$, its Helgason-Fourier transform is defined by

$$\widetilde{f}(\rho,b) = \int_{\mathbb{D}} f(z)e_{-\rho,b}(z)\mathrm{dm}(z),\quad \forall(\rho,b)\in\mathbb{R}\times\partial\mathbb{D} \tag{4.5}$$

Assuming that $U(\mathbf{r},z) = e^{i\mathbf{k}\cdot\mathbf{r}}e_{\rho,b}(z)$ we obtain the following relation

$$\sigma = -1+\mu s_1\left(\widetilde{W}_{loc}(\rho)+\beta\widehat{\mathcal{J}}(q)\widetilde{\mathcal{K}}(\rho)\right) \tag{4.6}$$

where $\widehat{\mathcal{J}}(q)$ is the Hankel transform of $\mathcal{J}(\|\cdot\|)$ with $q = \|\mathbf{k}\|$ and $\widetilde{W}_{loc}(\rho)$ (resp. $\widetilde{\mathcal{K}}(\rho)$) is the Helgason-Fourier transform of $W_{loc}(d_{\mathbb{D}}(\cdot,0))$ (resp. $\mathcal{K}(d_{\mathbb{D}}(\cdot,0))$). The fact that Helgason-Fourier transform of $W_{loc}(d_{\mathbb{D}}(\cdot,0))$ and $\mathcal{K}(d_{\mathbb{D}}(\cdot,0))$ does not depend upon $b\in\partial\mathbb{D}$ was already proved in [27]. It follows that the neutral stability curve

$$\mu(q,\rho) = \left(s_1\left(\widetilde{W}_{loc}(\rho)+\beta\widehat{\mathcal{J}}(q)\widetilde{\mathcal{K}}(\rho)\right)\right)^{-1}$$

attains its minimum at $\mu_c = \left(s_1\left(\widetilde{W}_{loc}(\rho_c)+\beta\widehat{\mathcal{J}}(q_c)\widetilde{\mathcal{K}}(\rho_c)\right)\right)^{-1}$ with (q_c,ρ_c) defined by $(q_c,\rho_c) = \max_{(q,\rho)\in\mathbb{R}^+\times\mathbb{R}}\left[\widetilde{W}_{loc}(\rho)+\beta\widehat{\mathcal{J}}(q)\widetilde{\mathcal{K}}(\rho)\right]$.

A consequence of the $\mathbf{E}(2)\times\mathbf{U}(1,1)$ symmetry is that the kernel of the linearized equation (4.2), at the critical point $\mu=\mu_c$ is infinite dimensional (indifference to

b and all $\mathbf{k}$ such that $\|\mathbf{k}\| = q_c$). As in the Euclidean case of pattern formation, we want to look for solutions in the restricted class of patterns which are doubly periodic in the $\mathbf{r}$ variable and spatially periodic in the z variable. Doubly-periodic functions on the Euclidean plane correspond to rectangular, square and hexagonal tilings of $\mathbb{R}^2$, see section 3.3.2. Functions which are periodic in the Poincaré disk $\mathbb{D}$ are, by definition, invariant under the action of a discrete subgroup $\mathbf{G}$ of $\mathbf{U}(1,1)$ whose fundamental domain is a polygon. Such a subgroup is called a cocompact Fuchsian group and we can restrict further to look for such groups which contain no elliptic elements nor reflections[1].

Tilings of the Poincaré disc have very different properties from tilings of the Euclidean plane. In particular tilings exist with polygons having an arbitrary number of sides, while in $\mathbb{R}^2$ only rectangular, square and hexagonal periodic tilings exist. But the size of a regular polygon with a given number of vertices is fixed in hyperbolic geometry, a consequence of the Gauss-Bonnet formula [40]. This has for consequence to render discrete the set of values of the wave number ρ_c and hence μ_c. It follows that, although we can look for the bifurcation of spatially periodic solutions associated with a given tessellation in $\mathbb{D}$, these patterns will not in general correspond to the most unstable perturbations unless the parameters in the equation are tuned so that it happens this way. In section 4.3, we will tune the parameters of the local connectivity function W_{loc}, such that the most unstable mode is associated to the tiling that we have chosen.

This problem of pattern formation on the Poincré disk was presented in [18, 26] and an example was studied, namely the case where the group $\mathbf{G}$ corresponds to a tiling of $\mathbb{D}$ with regular octagons. This particular choice was initially motivated and explained in [20] where families of subgroups of $\mathbf{U}(1,1)$ were identified to naturally arise from the retinal input to the hypercolumns in the visual area V1 such as the group $\mathbf{G}$. In this case $\mathbf{G}$ is generated by four hyperbolic transformations which are rotated from each other by angles $k\pi/4$ ($k = 1, 2, 3$), and $\mathbb{D}/\Gamma$ is a double torus (genus 2 surface). Moreover the group of automorphisms $\mathcal{G}$ of $\mathbb{D}/\mathbf{G}$ is known and has 96 elements. Restricting to the class of $\mathbf{G}$-periodic functions, the initial bifurcation problem is now reduced to an equation that is invariant under the action of $\mathcal{G}$. By standard center manifold reduction, this equation can be projected onto the critical eigenspace of the linearized operator. In our case the critical eigenvalue is 0 ("steady state" bifurcation) and its eigenspace is an absolutely irreducible representation space of the group $\mathcal{G}$.

4.2. **Bifurcations of octagonal H-planforms.** In this section, we introduce the octagonal lattice and its symmetries, we recall the structure of the group $\mathcal{G}$ of automorphisms of $\mathbb{D}/\mathbf{G}$ and its irreducible representations. We also recall the main result of [18, 26] about the bifurcation of H-planforms in this case.

4.2.1. *General setting.* The octagonal lattice group $\mathbf{G}$ is generated by the following four hyperbolic transformations (boosts), see [3]:

$$g_0 = \begin{pmatrix} 1+\sqrt{2} & \sqrt{2+2\sqrt{2}} \\ \sqrt{2+2\sqrt{2}} & 1+\sqrt{2} \end{pmatrix} \tag{4.7}$$

[1]These subgroups of $\mathbf{SU}(1,1)$ contain only hyperbolic elements and are the exact counterparts of discrete translation subgroups of $\mathbb{R}^p$. They are called "torsion-free" cocompact Fuchsian groups, see [40].

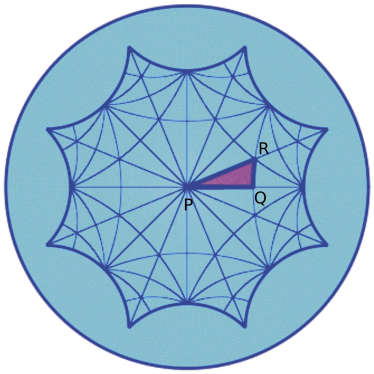

FIGURE 5. Tessellation of the hyperbolic octagon $\mathcal{O}$ with congruent triangles.

and $g_j = \mathrm{rot}_{j\pi/4} g_0 \mathrm{rot}_{-j\pi/4}$, $j = 1, 2, 3$, where rot_φ indicates the rotation of angle φ around the origin in $\mathbb{D}$. The fundamental domain of the lattice is a regular octagon $\mathcal{O}$ as shown in Figure 5. The opposite sides of the octagon are identified by periodicity, so that the corresponding quotient surface $\mathbb{D}/\mathbf{G}$ is isomorphic to a "double doughnut" (genus two surface) [3]. The fundamental octagon $\mathcal{O}$ can be further decomposed into 96 congruent triangles (see Figure 5) with angles $\pi/2$, $\pi/3$ and $\pi/8$. By applying reflections through the sides of one triangle (like the purple one in Figure 5) and iterating the process, applying if necessary a translation in $\mathbf{G}$ to get the resulting triangle back to $\mathcal{O}$, one fills out the octagon. The set of all these transformations (mod $\mathbf{G}$) is isomorphic to the group of automorphisms of $\mathbb{D}/\mathbf{G}$, we call it $\mathcal{G}$. Let us call P, Q, R the vertices of the red triangle in Figure 5 which have angles $\pi/8$, $\pi/2$ and $\pi/3$ respectively.

Definition 4.2. We set :
(i) κ, κ' and κ'' the reflections through the sides PQ, PR and QR respectively (mod $\mathbf{G}$);
(ii) ρ the rotation by $\pi/4$ centered at P, σ the rotation by π centered at Q and ϵ the rotation by $2\pi/3$ centered at R (mod $\mathbf{G}$).

Note that $\rho = \kappa'\kappa$, $\sigma = \kappa''\kappa$ and $\epsilon = \kappa''\kappa'$. Moreover $\rho\sigma\epsilon = Id$. Any two of these "rotations" generate the subgroup $\mathcal{G}_0$ of orientation-preserving automorphisms of $\mathcal{G}$. It can be seen that $\mathcal{G} = \mathcal{G}_0 \cup \kappa \cdot \mathcal{G}_0$, and moreover $\mathcal{G}_0$ can be identified with $\mathbf{GL}(2, 3)$, the group of invertible 2×2 matrices with entires in the field $\mathbb{Z}_3$.

There are 13 conjugacy classes and therefore 13 complex irreducible representations of $\mathcal{G}$, the characters of which will be denoted χ_j, $j = 1, ..., 13$. It was shown in [18] that there are 4 irreducible representations of dimension 1, 2 of dimension 2, 4 of dimension 3 and 3 of dimension 4. In the following we shall denote the irreducible representations by their character: χ_j is the representation with this character. The following lemma is proved in [18].

Lemma 4.3. *All the irreducible representations of $\mathcal{G}$ are real absolutely irreducible. In other words, any matrix which commutes with such a representation is a real scalar multiple of the identity matrix.*

4.2.2. *Irreducible representation χ_8.* For each representations χ_1 to χ_{13}, we have given in [18] the isotropy types of each representations which have on dimensional

fixed-point subspace and presented in [18, 26] the corresponding bifurcation diagrams. In this study, we focus on the case of the irreduclible representation χ_8. The choice of χ_8 is arbitrary for the moment but will be explained in great details in 4.2.4. In that case, from Theorem 5 in [18] and Theorem 1 in [26], we have the following proposition. We recall that the octahedral group $\mathbb{O}$, the direct symmetry group of the cube, possesses two irreducible representations of dimension three. In order to differentiate these two irreducible representations we adopt the convention "natural" as used in [48].

Proposition 4.1. *For the three dimensional irreducible representation χ_8 of $\mathcal{G}$, the isotropy subgroups with one dimensional fixed point subspace are the following:*

$$\begin{aligned}\mathbf{D}_8 &= \langle \rho, \kappa \rangle \\ \widetilde{\mathbf{C}}_{6\kappa'} &= \langle -\epsilon, \kappa' \rangle \\ \widetilde{\mathbf{D}}_{2\kappa} &= \langle -Id, \sigma, \kappa \rangle.\end{aligned}$$

The bifurcation diagram is the same as the bifurcation diagram with "natural" full octahedral $\mathbb{O} \ltimes \mathbb{Z}_2$ symmetry in $\mathbb{R}^3$.

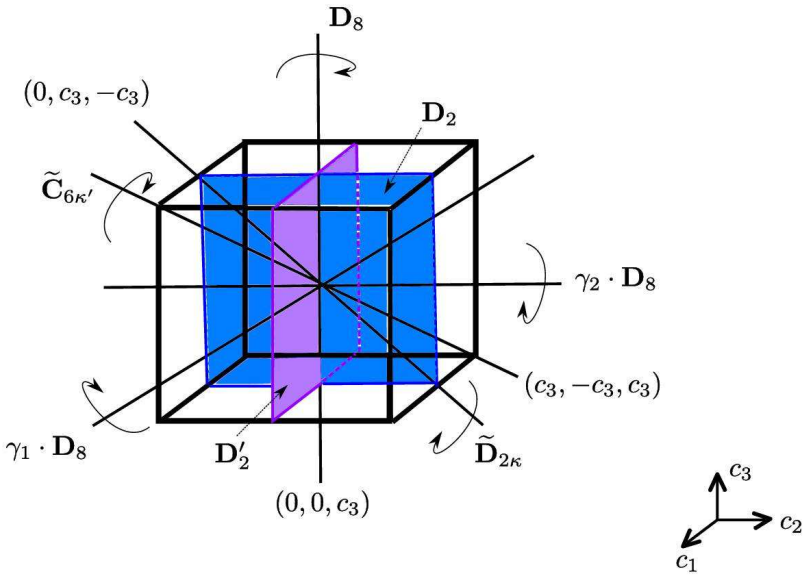

FIGURE 6. Maximal isotropy subgroups $\mathbf{D}_8, \widetilde{\mathbf{C}}_{6\kappa'}$ and $\widetilde{\mathbf{D}}_{2\kappa}$ of $\mathbb{O} \ltimes \mathbb{Z}_2$. The axes $\gamma_1 \cdot \mathbf{D}_8$ and $\gamma_2 \cdot \mathbf{D}_8$ are copies of $\mathbf{D}_8$ by the elements $\gamma_1, \gamma_2 \in \mathcal{G}$ (see 4.2.3). The plane $(0, c_2, c_3)$ (resp. $(c_1, 0, c_3)$) has symmetry $\mathbf{D}_2$ (resp. $\mathbf{D}_2'$).

4.2.3. *Associated octagonal H-planforms.* In order to illustrate our purpose, we numerically compute the octagonal H-planforms associated to the irreducible representation χ_8 of $\mathcal{G}$. We recall that these planforms are eigenfunctions of the Laplace-Beltrami operator in $\mathbb{D}$, defined in equation (4.4), which satisfy certain isotropy conditions: (i) being invariant under a lattice group $\mathbf{G}$ and (ii) being invariant under the action of an isotropy subgroup of the symmetry group of the fundamental domain $\mathbb{D}/\mathbf{G}$ (mod $\mathbf{G}$). We implement the finite element method (see [21] for a review) with periodic boundary conditions in the octagon and afterward, identify the corresponding planforms. Our results are in agreement with those of Aurich and Steiner reported in [1]. In figure 7, we plot the corresponding eigenfunctions of the Laplace-Beltrami operator associated to the lowest non-negative eigenvalue $\lambda = 3.8432$ with multiplicity 3. We identify each solution by its symmetry group. Note that the solution in figure 7(a) corresponds to an axis of symmetry in the sense that its symmetry group is an isotropy subgroup with one dimensional fixed point subspace. In figure 8, we plot each eigenfunction in the Poincaré disk. It becomes now clear that 8(b) and 8(c) can be obtained from 8(a) by hyperbolic transformations. From appendix B and the definition of g_0 in equation (4.7), we see that $g_0 = a_{r_0}$ with $r_0 = \ln\left(1+\sqrt{2}+\sqrt{2+\sqrt{2}}\right)$. If we define $\gamma_k \in \mathcal{G}$ by:

$$\gamma_k = \mathrm{rot}_{k\pi/4} a_{r_0/2} \mathrm{rot}_{-k\pi/4}$$

then figure 8(b) (resp. 8(c)) is obtained from 8(a) by applying γ_1 (resp. γ_2). Planforms in figure 8 correspond the three coordinate axes of the cube in figure 6.

4.2.4. *Polar map and choice of* χ_8. In optical imaging ([17] for a review), a polar map is obtained by combining the color code for preferred orientation with a brightness code representing the strength of orientation tuning. Dark regions represent areas of weak tuning, whereas bright areas represent strong orientation preference. Dark areas are prevalent in pinwheel centers. The **PM** is a functional map that assigns each location $\mathbf{r}$, a complex number $z(\mathbf{r})$. The values of $z(\mathbf{r})$ are calculated from the **OM** as follows. Let $(\varphi_j)_{j=1\ldots p}$ be p equidistant orientations presented to the animal, let $S_{\mathbf{r}}^{\varphi_j}$ denote the response at location $\mathbf{r}$ for the **OM** evoked by orientation φ_j.

$$z(\mathbf{r}) = \rho(\mathbf{r}) e^{i\theta(\mathbf{r})} = \frac{2}{p} \sum_{j=1}^{p} S_{\mathbf{r}}^{\varphi_j} e^{i\varphi_j}$$

where $\theta(\mathbf{r})$ is the preferred orientation at location $\mathbf{r}$ and the magnitude measures the degree to which the response at location $\mathbf{r}$ is modulated by the stimulus's orientation. This is the *selectivity* of location $\mathbf{r}$. When moving from a point far from the pinwheel towards the pinwheel, the selectivity is gradually reduced, resulting in a large range of selectivity values. For each preferred orientation there is a wide range of selectivities. It was shown in [59] that neurons in regions of homogeneous orientation preference (iso-orientation domains) have much sharper tuning than in heterogeneous regions of the map (near pinwheel centers). These anatomical experiments lead us to identify a point of the polar map $z(\mathbf{r})$ with a point in the Poincaré disk seen as a structure tensor of determinant equal one. The point $z = 0$ of the Poincaré disk is interpreted as a point where all orientations are represented with low selectivity and then corresponds to a pinwheel center, whereas a point $z = |z|e^{i\theta}$ close the boundary $\mathbb{D}$ has a preferred orientation θ and a very high selectivity.

We have identified the modulus of a point in the Poincaré disk to the selectivity. From the computer vision point of view, the modulus can also be linked to to the

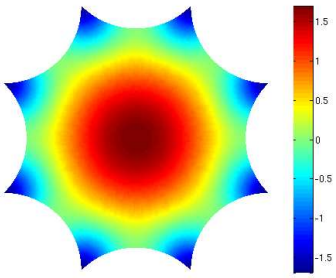

(a) Symmetry $\mathbf{D}_8 =< \rho, \kappa >$.

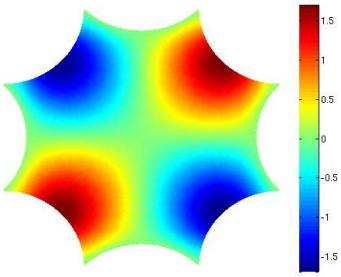

(b) Symmetry $\mathbf{D}'_2 =< -Id, \rho^2\kappa >$.

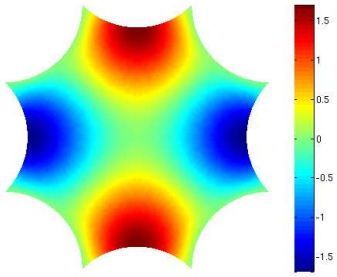

(c) Symmetry $\mathbf{D}_2 =< -Id, \kappa >$.

FIGURE 7. Plot of the eigenfunctions of the Laplace-Beltrami operator in the octagon $\mathcal{O}$ associated to the lowest non-negative eigenvalue $\lambda = 3.8432$ corresponding to the irreducible representation χ_8.

coherence of the corresponding structure tensor. The coherence measures the degree of anisotropy of the two eigenvalues of the structure tensor. For a given structure tensor $\mathcal{T}$, the coherence is defined as the ratio $\frac{\lambda_1-\lambda_2}{\lambda_1+\lambda_2}$, where $\lambda_1 \geq \lambda_2 > 0$ are the two eigenvalues of $\mathcal{T}$. In the case of a structure tensor $\mathcal{T}$ with determinant equal to 1 which is identified to a point $z \in \mathbb{D}$, we have $\frac{\lambda_1-\lambda_2}{\lambda_1+\lambda_2} = \frac{2|z|}{1+|z|^2}$. Then the coherence is directly linked to the selectivity.

The choice of irreducible representation χ_8 comes from the direct interpretation of H-planforms plotted in figures 7(b), 7(c) and 7(a) in terms of preferred orientation. For example, in figure 7(a), the high region of activity near the center of the Poincaré disk traduces the fact the point $z = 0$ is preferred, this means that the selectivity is low and all orientations are represented. On the other hand, in figure 7(b), two points on the boundary of the octagon correspond to high activity of the eigenfunction. Due to the periodicity (opposite faces of the octagon are identified), these two points are the same and thus there is a preferred orientation at $\frac{\pi}{4}$. With a similar argument, in figure 7(c), there is a preferred orientation at $\frac{\pi}{2}$. As surprising as it can be, solutions in figures 7(b), 7(c) and 7(a) have to be thought as unimodal solution of the z variable due to the periodicity. These solutions are the

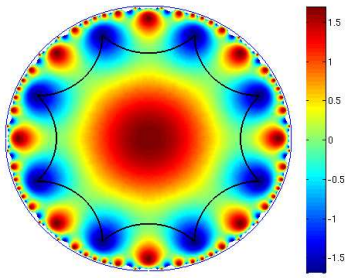

(a) H-planform Ψ_3 with symmetry $\mathbf{D}_8$.

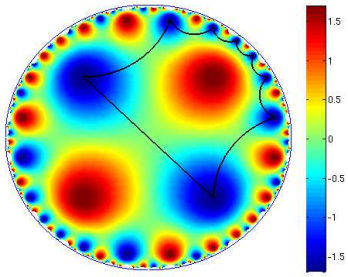

(b) H-planform Ψ_1 with symmetry $\gamma_1 \cdot \mathbf{D}_8$.

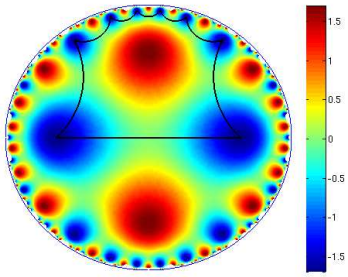

(c) H-planform Ψ_2 with symmetry $\gamma_2 \cdot \mathbf{D}_8$.

FIGURE 8. Plot of the eigenfunctions of the Laplace-Beltrami operator in the Poincaré disk $\mathbb{D}$ associated to the lowest non-negative eigenvalue $\lambda = 3.8432$ corresponding to the irreducible representation χ_8. In (a) we also plot the octagon (black line) and in (b),(c) its image by γ_1, γ_2 respectively.

counterpart, in the hyperbolic disk, to the tuning curves found in the ring model of orientations [4, 30].

4.3. **Bifurcation diagrams for one hypercolumn.** In this paragraph, we consider the case $\beta = 0$ and deal with the following equation:

$$\frac{\partial V(z,t)}{\partial t} = -V(z,t) + \int_{\mathbb{D}} W_{loc}\left(d_{\mathbb{D}}(z,z')\right) S(\mu V(z',t)) \mathrm{dm}(z'). \tag{4.8}$$

For $S(0) = 0$, the fully symmetric state $V = 0$ is always solution of (4.8) and the associated linear equation is given by

$$\frac{\partial V(z,t)}{\partial t} = -V(z,t) + \mu s_1 \int_{\mathbb{D}} W_{loc}\left(d_{\mathbb{D}}(z,z')\right) V(z',t) \mathrm{dm}(z'). \tag{4.9}$$

If we denote Ψ_1 the H-planform in figure 7(b), Ψ_2 the H-planform in figure 7(c) and Ψ_3 the H-planform corresponding to the symmetry group $\mathbf{D}_8$ in figure 7(a), then (Ψ_1, Ψ_2, Ψ_3) is a basis for the irreducible representation χ_8. This can be easily seen through the identification of each H-planform to the three coordinate axes of the

cube in figure 6. Then if we define:

$$\frac{1}{4\pi}\int_{\mathcal{O}}\int_{\mathbb{D}} W_{loc}\left(d_{\mathbb{D}}(z,z')\right)\Psi_i(z)\Psi_i(z')\mathrm{dm}(z')\mathrm{dm}(z) = \widetilde{W}^c_{loc} \quad \forall i = 1\dots 3$$

there is a bifurcation at $\mu_c = \left(s_1\widetilde{W}^c_{loc}\right)^{-1}$ such that for $\mu < \mu_c$ the state $V = 0$ is stable. Note that we have normalized planforms such that:

$$\langle \Psi_i, \Psi_j\rangle = \frac{1}{4\pi}\int_{\mathcal{O}} \Psi_i(z)\Psi_j(z)\mathrm{dm}(z) = \delta_{i,j}.$$

If we rewrite equation (4.8) as

$$V' = \mathbf{L}V + \mathcal{R}(V,\lambda)$$

with $\lambda = \mu - \mu_c$ and

$$\begin{aligned}\mathbf{L}V &= -V + \mu_c s_1 W_{loc}\star V\\ \mathcal{R}(V,\lambda) &= W_{loc}\star\left(S((\lambda+\mu_c)V) - \mu_c s_1 V\right).\end{aligned}$$

Close to the bifurcation point, there exists a polynomial map $\Phi(\cdot,\lambda)$ such that the change of variable:

$$V(z) = c_1\Psi_1 + c_2\Psi_2 + c_3\Psi_3 + \Phi(c_1,c_2,c_3,\lambda)$$

transforms equation (4.8) into the normal form (see [47] for a review on bifurcation problems with octahedral symmetry):

$$\left\{\begin{array}{rcl}\frac{dc_1}{dt} &=& \frac{\lambda}{\mu_c}c_1 + \left[a(c_2^2+c_3^2) + bc_1^2\right]c_1 + \text{h.o.t.}\\ \frac{dc_2}{dt} &=& \frac{\lambda}{\mu_c}c_2 + \left[a(c_1^2+c_3^2) + bc_2^2\right]c_2 + \text{h.o.t.}\\ \frac{dc_3}{dt} &=& \frac{\lambda}{\mu_c}c_3 + \left[a(c_1^2+c_2^2) + bc_3^2\right]c_3 + \text{h.o.t.}\end{array}\right. \tag{4.10}$$

Taylor expanding the map Φ:

$$\Phi(c_1,c_2,c_3,\lambda) = \sum_{1\le r+s+l+m\le 3} c_1^r c_2^s c_3^l \lambda^m \Phi_{rslm}$$

and $\mathcal{R}$:

$$\mathcal{R}(V,\lambda) = \mathcal{R}_{11}(V,\lambda) + \mathcal{R}_{20}(V,V) + \mathcal{R}_{30}(V,V,V) + \text{h.o.t.}$$

with

$$\begin{aligned}\mathcal{R}_{11}(V,\lambda) &= \lambda s_1 W_{loc}\star V\\ \mathcal{R}_{20}(U,V) &= \frac{\mu_c^2 s_2}{2}W_{loc}\star(UV)\\ \mathcal{R}_{300}(U,V,W) &= \frac{\mu_c^3 s_3}{6}W_{loc}\star(UVW)\end{aligned}$$

where $s_2 = S''(0)$ and $s_3 = S'''(0)$ we obtain the following system of equations:

$$\begin{aligned}0 &= -\mathbf{L}\Phi_{0020} - \mathcal{R}_{20}(\Psi_3,\Psi_3)\\ 0 &= -\mathbf{L}\Phi_{1010} - 2\mathcal{R}_{20}(\Psi_1,\Psi_3)\\ a &= \langle 2\mathcal{R}_{20}(\Phi_{0020},\Psi_1) + 2\mathcal{R}_{20}(\Phi_{1010},\Psi_3) + 3\mathcal{R}_{30}(\Psi_1,\Psi_3,\Psi_3),\Psi_1\rangle\\ b &= \langle 2\mathcal{R}_{20}(\Psi_3,\Phi_{0020}) + \mathcal{R}_{30}(\Psi_3,\Psi_3,\Psi_3),\Psi_3\rangle.\end{aligned} \tag{4.11}$$

In order to solve the two first equations of the previous system, we need to know the functions $\Psi_3(z)\Psi_3(z)$ and $\Psi_1(z)\Psi_3(z)$ can be expressed as a linear combination of eigenfunctions of the Laplace-Beltrami operator on $\mathcal{O}$. In general, it is very

difficult to obtain these expressions because the eigenfunctions are only know numerically and one needs the computation of the associated Clebsch-Gordan coefficients. It turns out that in our case we have been able to conjecture and numerically verify the following relations:

$$\Psi_1(z)\Psi_3(z) = \frac{1}{\sqrt{3}}\Psi_{\chi_{10}}^{\mathbf{D}'_{2\kappa}}(z)$$
$$\Psi_3^2(z) = \frac{6}{5}\Psi_{\chi_6}^{\widetilde{\mathbf{D}}_{8\kappa}}(z) + 1$$

where the corresponding isotropy subgroups are given by:

$$\mathbf{D}'_{2\kappa} =< -Id, \rho^2\kappa, \rho^2\sigma > \text{ and } \widetilde{\mathbf{D}}_{8\kappa} =< \rho, \rho^2\sigma\rho^{-2}, \kappa > .$$

Furthermore we have normalized $\Psi_{\chi_{10}}^{\mathbf{D}'_{2\kappa}}$ and $\Psi_{\chi_6}^{\widetilde{\mathbf{D}}_{8\kappa}}$ such that:

$$\langle \Psi_{\chi_{10}}^{\mathbf{D}'_{2\kappa}}, \Psi_{\chi_{10}}^{\mathbf{D}'_{2\kappa}} \rangle = \langle \Psi_{\chi_6}^{\widetilde{\mathbf{D}}_{8\kappa}}, \Psi_{\chi_6}^{\widetilde{\mathbf{D}}_{8\kappa}} \rangle = 1.$$

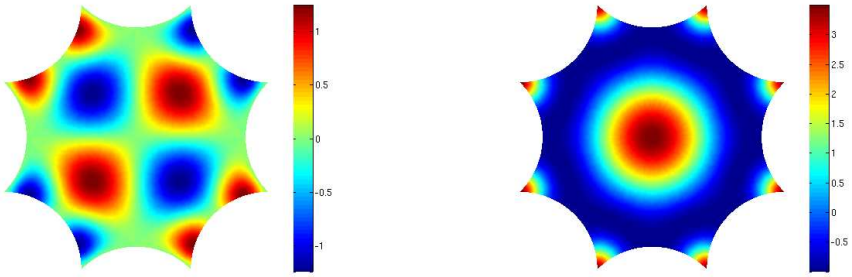

(a) Plot of $\Psi_{\chi_{10}}^{\mathbf{D}'_{2\kappa}}$.

(b) Plot of $\Psi_{\chi_6}^{\widetilde{\mathbf{D}}_{8\kappa}}$.

FIGURE 9. Plot of the eigenfunctions of the Laplace-Beltrami operator in the octagon $\mathcal{O}$ corresponding to the irreducible representations χ_{10} with eigenvalue $\lambda = 15.0518$ (left) and χ_6 with eigenvalue $\lambda = 8.2501$ (right).

In figure 9, we plot the eigenfunctions $\Psi_{\chi_{10}}^{\mathbf{D}'_{2\kappa}}$ and $\Psi_{\chi_6}^{\widetilde{\mathbf{D}}_{8\kappa}}$ of the Laplace-Beltrami operator in the octagon $\mathcal{O}$. One interesting remark is that the product $\Psi_1\Psi_3$ corresponding to the three dimensional irreducible representation χ_8 produces an eigenfunction associated to another three dimensional irreducible representation: χ_{10} whereas Ψ_3^2 is the linear combination of the constant function which has $\mathcal{G}$ as isotropy subgroup and thus corresponds to χ_1 and the eigenfunction $\Psi_{\chi_6}^{\widetilde{\mathbf{D}}_{8\kappa}}$ which is associated to two dimensional irreducible representation χ_6.

If we define

$$\widetilde{W}_{loc}^{\chi_{10},\mathbf{D}'_{2\kappa}} = \frac{1}{4\pi}\int_{\mathcal{O}}\int_{\mathbb{D}} W_{loc}\left(d_{\mathbb{D}}(z,z')\right)\Psi_{\chi_{10}}^{\mathbf{D}'_{2\kappa}}(z)\Psi_{\chi_{10}}^{\mathbf{D}'_{2\kappa}}(z')\mathrm{dm}(z')\mathrm{dm}(z)$$
$$\widetilde{W}_{loc}^{\chi_6,\widetilde{\mathbf{D}}_{8\kappa}} = \frac{1}{4\pi}\int_{\mathcal{O}}\int_{\mathbb{D}} W_{loc}\left(d_{\mathbb{D}}(z,z')\right)\Psi_{\chi_6}^{\widetilde{\mathbf{D}}_{8\kappa}}(z)\Psi_{\chi_6}^{\widetilde{\mathbf{D}}_{8\kappa}}(z')\mathrm{dm}(z')\mathrm{dm}(z)$$
$$\widetilde{W}_{loc}^{\chi_1} = \int_{\mathbb{D}} W_{loc}\left(d_{\mathbb{D}}(z,z')\right)\mathrm{dm}(z')$$

then the two first equations of system (4.11) give

$$\Phi_{0020} = \mathrm{Span}\,(\Psi_1,\Psi_2,\Psi_3) + \frac{\mu_c^2 s_2}{2}\left[\frac{\widetilde{W}_{loc}^{\chi_1}}{1-\widetilde{W}_{loc}^{\chi_1}/\widetilde{W}_{loc}^{c}} + \frac{6}{5}\frac{\widetilde{W}_{loc}^{\chi_6,\widetilde{\mathbf{D}}_{8\kappa}}}{1-\widetilde{W}_{loc}^{\chi_6,\widetilde{\mathbf{D}}_{8\kappa}}/\widetilde{W}_{loc}^{c}}\Psi_{\chi_6}^{\widetilde{\mathbf{D}}_{8\kappa}}\right]$$

$$\Phi_{1010} = \mathrm{Span}\,(\Psi_1,\Psi_2,\Psi_3) + \frac{\mu_c^2 s_2}{\sqrt{3}}\frac{\widetilde{W}_{loc}^{\chi_{10},\mathbf{D}'_{2\kappa}}}{1-\widetilde{W}_{loc}^{\chi_{10},\mathbf{D}'_{2\kappa}}/\widetilde{W}_{loc}^{c}}\Psi_{\chi_{10}}^{\mathbf{D}'_{2\kappa}}.$$

We can now obtain the expression of the coefficients a and b in the reduced equation (4.10).

Lemma 4.4.

$$\begin{aligned} a = \mu_c^3 W_{loc}^c\Bigg(&\frac{s_3}{6} + \frac{\mu_c s_2^2}{2}\left[\frac{\widetilde{W}_{loc}^{\chi_1}}{1-\widetilde{W}_{loc}^{\chi_1}/\widetilde{W}_{loc}^{c}} - \frac{2}{3}\frac{\widetilde{W}_{loc}^{\chi_6,\widetilde{\mathbf{D}}_{8\kappa}}}{1-\widetilde{W}_{loc}^{\chi_6,\widetilde{\mathbf{D}}_{8\kappa}}/\widetilde{W}_{loc}^{c}}\right.\\ &\left.+\frac{1}{3}\frac{\widetilde{W}_{loc}^{\chi_{10},\mathbf{D}'_{2\kappa}}}{1-\widetilde{W}_{loc}^{\chi_{10},\mathbf{D}'_{2\kappa}}/\widetilde{W}_{loc}^{c}}\right]\Bigg) \end{aligned} \tag{4.12}$$

$$b = \mu_c^3 W_{loc}^c\left(\frac{61 s_3}{150} + \frac{\mu_c s_2^2}{2}\left[\frac{\widetilde{W}_{loc}^{\chi_1}}{1-\widetilde{W}_{loc}^{\chi_1}/\widetilde{W}_{loc}^{c}} + \frac{36}{25}\frac{\widetilde{W}_{loc}^{\chi_6,\widetilde{\mathbf{D}}_{8\kappa}}}{1-\widetilde{W}_{loc}^{\chi_6,\widetilde{\mathbf{D}}_{8\kappa}}/\widetilde{W}_{loc}^{c}}\right]\right). \tag{4.13}$$

Proof. See appendix D. □

From the analysis derived in [47], we have the following result.

Lemma 4.5. *The stability of the branches of solutions corresponding to the three maximal isotropy subgroups given in proposition 4.1 is:*

(i) the $\mathbf{D}_8$ *branch is stable if and only if* $a < b < 0$,
(ii) the $\widetilde{\mathbf{C}}_{6\kappa'}$ *branch is stable if and only if* $2a + b < 0$ *and* $b - a < 0$,
(iii) the $\widetilde{\mathbf{D}}_{2\kappa}$ *branch is never stable.*

The corresponding bifurcation diagram is given in figure 10 for $a < b < 0$.

We want that our hypercolumn produces tuning surfaces close the bifurcation point $\mu = \mu_c$. From the discussion made in paragraph 4.2.4 on the interpretation of H-planforms, we impose that the condition $a < b < 0$ is satisfied such that the $\mathbf{D}_8$ branch is the only stable branch. Depending on the initial condition in the (c_1, c_2, c_3)-space, the solution will converge to one of three axis of coordinates: $\mathbf{D}_8, \gamma_1 \cdot \mathbf{D}_8$ or $\gamma_2 \cdot \mathbf{D}_8$. The condition $a < b < 0$ gives a constrain on the threshold T of the sigmoidal function defined in equation (2.2) and the different coefficients $\widetilde{W}_{loc}$ of the coupling function W_{loc}.

In order to illustrate this constrain on the parameters, we present a specific example. The local coupling function is given by:

$$W_{loc}(x) = A\cosh(2x)^{-\sigma_0} - \cosh(2x)^{-\sigma} \tag{4.14}$$

with $A > 1$ and $\sigma_0 > \sigma > \frac{1}{2}$. The Helgason-Fourier transform of $z \to W_{loc}(d_{\mathbb{D}}(z,0))$ can be computed analytically [62] and we have shown [27] that it only depends upon $\rho \in \mathbb{R}$ in definition 4.5:

$$\widetilde{W}_{loc}(\rho) = \sqrt{\pi}\left[A\frac{2^{\sigma_0-3}}{\Gamma(\sigma_0)}\left|\Gamma\left(\frac{\sigma_0 + i\rho - \frac{1}{2}}{2}\right)\right|^2 - \frac{2^{\sigma-3}}{\Gamma(\sigma)}\left|\Gamma\left(\frac{\sigma + i\rho - \frac{1}{2}}{2}\right)\right|^2\right]. \tag{4.15}$$

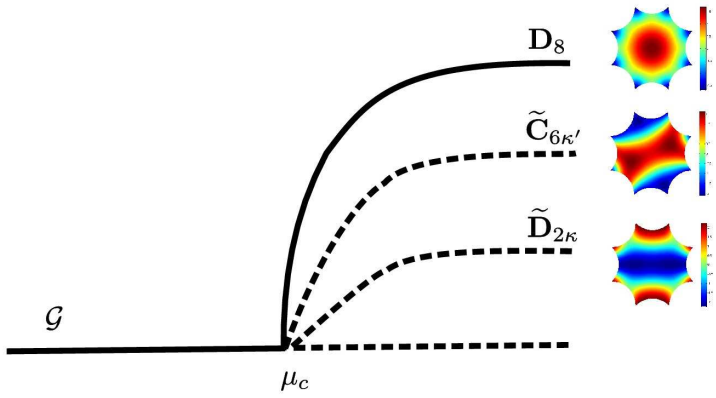

FIGURE 10. Bifurcation diagram in the case $a < b < 0$. Solid lines correspond to stable branches, dotted ones to unstable branches. For each maximal isotropy subgroups, we plot the corresponding planform.

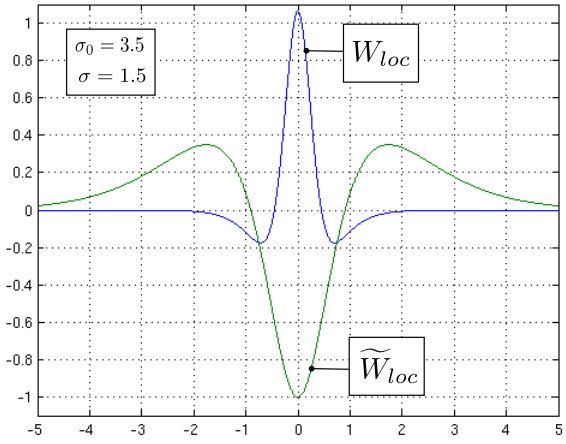

FIGURE 11. Plot of the local coupling function W_{loc} given in equation (4.14) and its Helgason-Fourier transform $\widetilde{W}_{loc}$ given in equation (4.14) with $\sigma_0 = 3.5$ and $\sigma = 1.5$. For the choice of A, see text.

Firstly, we fix the value of $\sigma_0 = 3.5$. Then, we tune the value of A such that the most unstable mode $\rho_c = \max_{\rho\in\mathbb{R}} \widetilde{W}_{loc}(\rho)$ corresponds to the irreducible representation χ_8. Note that A depends upon (σ_0, σ). In figure 11, we plot both the local connectivity function and its Helgason-Fourier transform for $\sigma = 1.5$. For each

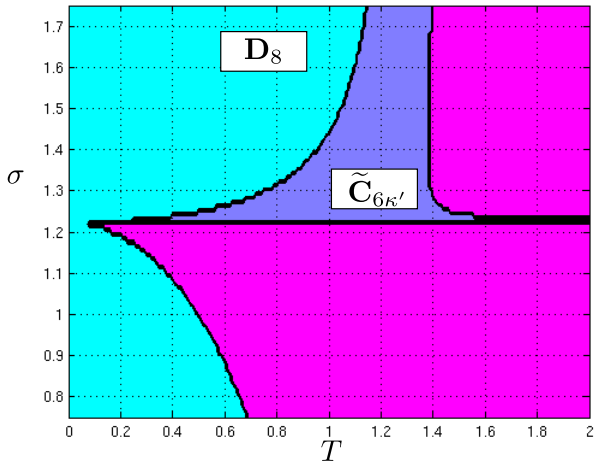

FIGURE 12. Regions of the plane (T, σ) where the branches $\mathbf{D}_8$ and $\widetilde{\mathbf{C}}_{6\kappa'}$ are stable with $\sigma_0 = 3.5$.

value of (T, σ) in $[0, 2] \times [0.75, 1.75]$ we have numerically computed the coefficients a and b given in lemma 4.4 and then checked if the stability conditions in lemma 4.5 are satisfied. Our results are plotted in figure 12. We can see the different regions of the plane (T, σ) where the branches $\mathbf{D}_8$ and $\widetilde{\mathbf{C}}_{6\kappa'}$ are stable: in blue the region where $\mathbf{D}_8$ is stable and in purple the region where $\widetilde{\mathbf{C}}_{6\kappa'}$ is stable.

4.4. **Symmetry-breaking bifurcations on lattices.** Knowing the behaviour of our network at the hypercolumnar level, we can come back to the fully isotropically connected model and we restrict ourselves to doubly periodic functions on a square lattice for the $\mathbf{r}$ variable and periodic on the octagon $\mathcal{O}$ in the z variable. The choice of the square lattice is dictated by the fact that the rotations of $\pi/2$ centered at 0 in the Euclidean square and of π at 0 in the hyperbolic octagon can be identified. Indeed, for anisotropic coupling, the action of a rotation on $(\mathbf{r}, z)$ is given by (see equation (2.9))

$$\mathcal{R}_\theta \cdot (\mathbf{r}, z) = \left(\mathcal{R}_\theta \mathbf{r}, e^{2i\theta} z\right)$$

so that if $\mathcal{O}$ is the feature space, only rotations with angle $\theta = k\frac{\pi}{4}$ are allowed. Hence the hexagonal lattice is not compatible with the octagonal tiling whereas both rhombic and square lattices are compatible.

By restricting the bifurcation problem to a direct product of lattices, the group of symmetries $\mathbf{E}(2) \times \mathbf{U}(1, 1)$ is transformed to the compact group $\Gamma \stackrel{def}{=} (\mathbf{D}_4 \ltimes \mathbb{T}^2) \times \mathcal{G}$, where $\mathbf{D}_4$ is the holohedry of the square lattice, $\mathbb{T}^2$ is the 2-torus (see paragraph 3.3.2) and $\mathcal{G}$ is the group of automorphisms of the octagon $\mathcal{O}$. The kernel of the linearized equation (4.2), at the critical point $\mu = \mu_c$ is now finite dimensional and tools from equivariant bifurcation theory can be applied. Namely, the Equivariant Branching Lemma [29, 19] ensures the existence of branches of equilibria for every axial subgroup of Γ and the remaining paragraphs will be dedicated to this study.

4.5. **Group actions.** As the principal isotropy subgroup for χ_8 is $\mathbf{C}_2 =< Id, -Id >$ we get a faithful action by taking $\mathcal{G}/\mathbf{C}_2 \cong \mathbb{O} \times \mathbf{Z}_2$, where $\mathbb{O}$ is the octahedral group.

By identifying elements of $\mathcal{G}$ with elements of the octahedral group $\mathbb{O}$ it is possible to construct action on the eigenspace spanned by Ψ_1, Ψ_2, Ψ_3. If we have:

$$u(z) = c_1\Psi_1(z) + c_2\Psi_2(z) + c_3\Psi_3(z)$$

we identify the eigenspace with $(c_1, c_2, c_3) \in \mathbb{R}^3$ and we have

$$\left\{\begin{array}{lcl} \rho \cdot (c_1, c_2, c_3) & = & (-c_2, c_1, c_3) \\ \kappa \cdot (c_1, c_2, c_3) & = & (-c_1, c_2, c_3) \\ \sigma \cdot (c_1, c_2, c_3) & = & (-c_1, -c_3, -c_2) \\ \epsilon \cdot (c_1, c_2, c_3) & = & (-c_2, -c_3, c_1) \end{array}\right.$$

where ρ, κ, σ and ϵ have been defined in 4.2.

We denote ξ the rotation of angle of $\pi/2$ centered at 0 of the square, δ the reflection along the horizontal axis and

$$\Theta = \theta_1\ell_1 + \theta_2\ell_2 \stackrel{def}{=} [\theta_1, \theta_2] \tag{4.16}$$

with $(\theta_1, \theta_2) \in [0, 2\pi[^2$. We suppose that the critical eigenspace $\mathcal{W}$ consists of functions of the form:

$$\begin{aligned} a(\mathbf{r}, z) = &\left(c_1\Psi_1(z) + c_2\Psi_2(z) + c_3\Psi_3(z)\right) e^{i\mathbf{k}_1\cdot\mathbf{r}} \\ &+ \left(d_1\Psi_1(z) + d_2\Psi_2(z) + d_3\Psi_3(z)\right) e^{i\mathbf{k}_2\cdot\mathbf{r}} + \text{c.c} \end{aligned} \tag{4.17}$$

where $(c_1, c_2, c_3, d_1, d_2, d_3) \in \mathbb{C}^6$. We will identify $\mathcal{W}$ with $\mathbb{C}^6$ through 4.17.

The action of ξ on $a(\mathbf{r}, z)$ can be expressed as:

$$\begin{aligned} \xi \cdot a(\mathbf{r}, z) &= a(\xi^{-1}\mathbf{r}, z) \\ &= \left(c_1\Psi_1(z) + c_2\Psi_2(z) + c_3\Psi_3(z)\right) e^{i\mathbf{k}_1\cdot\xi^{-1}\mathbf{r}} \\ &\quad + \left(d_1\Psi_1(z) + d_2\Psi_2(z) + d_3\Psi_3(z)\right) e^{i\mathbf{k}_2\cdot\xi^{-1}\mathbf{r}} + \text{c.c} \\ &= \left(\bar{d}_1\Psi_1(z) + \bar{d}_2\Psi_2(z) + \bar{d}_3\Psi_3(z)\right) e^{i\mathbf{k}_1\cdot\mathbf{r}} \\ &\quad + \left(c_1\Psi_1(z) + c_2\Psi_2(z) + c_3\Psi_3(z)\right) e^{i\mathbf{k}_2\cdot\mathbf{r}} + \text{c.c}\ . \end{aligned}$$

Then we have $\xi \cdot (c_1, c_2, c_3, d_1, d_2, d_3) = (\bar{d}_1, \bar{d}_2, \bar{d}_3, c_1, c_2, c_3)$ and the action of each elements on $(c_1, c_2, c_3, d_1, d_2, d_3)$ is given by

$$\left\{\begin{array}{lcl} \xi \cdot (c_1, c_2, c_3, d_1, d_2, d_3) & = & (\bar{d}_1, \bar{d}_2, \bar{d}_3, c_1, c_2, c_3) \\ \delta \cdot (\quad\ '' \quad\ ) & = & (c_1, c_2, c_3, \bar{d}_1, \bar{d}_2, \bar{d}_3,) \\ \Theta \cdot (\quad\ '' \quad\ ) & = & (e^{-i2\pi\theta_1}(c_1, c_2, c_3), e^{-i2\pi\theta_2}(d_1, d_2, d_3)) \\ \rho \cdot (\quad\ '' \quad\ ) & = & (-c_2, c_1, c_3, -d_2, d_1, d_3) \\ \kappa \cdot (\quad\ '' \quad\ ) & = & (-c_1, c_2, c_3, -d_1, d_2, d_3) \\ \sigma \cdot (\quad\ '' \quad\ ) & = & (-c_1, -c_3, -c_2, -d_1, -d_3, -d_2) \\ \epsilon \cdot (\quad\ '' \quad\ ) & = & (-c_2, -c_3, c_1, -d_2, -d_3, d_1). \end{array}\right. \tag{4.18}$$

Lemma 4.6. *The action of Γ on $\mathbb{C}^6$, given in 4.18, is absolutely irreducible.*

Proof. Any 6×6 complex matrix which commutes with the action $\mathbf{D}_4 \ltimes \mathbb{T}^2$ decomposes into a direct sum of two 3×3 identical diagonal matrices with real entries. Indeed the action of translations forces any 6×6 complex matrix to be diagonal with real entries and the action of $\mathbf{D}_4$ decomposes this matrix into two 3×3 identical diagonal matrices. The action of $\mathcal{G}$ renders each diagonal matrix equal to a scalar multiple of the identity matrix $\mathbb{I}_3$, which proves that the action of Γ is absolutely irreducible. Note that we could also have directly apply the general result of lemma 4.7 in order to prove this lemma. □

Our aim is now to apply the Equivariant Branching Lemma (see [29]). For this, we need to compute each isotropy subgroup Σ of Γ such that the subspace $\mathcal{W}^{\Sigma} = \{x \in \mathcal{W} \mid \Sigma \cdot x = x\}$ is one dimensional. Such subgroups are called axial. We recall the following lemma, the proof of which is given in Serre [60].

Lemma 4.7. *Let $H = H_1 \times H_2$ be an isotropy subgroup for the irreducible representation R of $G_1 \times G_2$ acting in X. Then $X = X_1 \otimes X_2$ and $R = R_1 \otimes R_2$ where R_1 is an irreducible representation of G_1 in V_1 and R_2 is an irreducible representation of G_2 in V_2 and therefore H_1 acts in V_1 and H_2 acts in V_2. Furthermore we have:*

$$dim\left(X^H\right) = 1 \text{ if and only if } dim\left(V_1^{H_1}\right) = dim\left(V_2^{H_2}\right) = 1.$$

It is then possible to determine the maximal isotropy subgroups of Γ that satisfy the hypotheses of the Equivariant Branching Lemma.

Theorem 4.8. *The following six isotropy subgroups are axial:*

- $\Sigma_1 = \mathbf{D}_4(\xi, \delta) \times \mathbf{D}_8$
- $\Sigma_2 = \left[\mathbf{O}_2(\xi^2, [0, \theta_2]) \times \mathbf{Z}_2(\delta)\right] \times \mathbf{D}_8$
- $\Sigma_3 = \mathbf{D}_4(\xi, \delta) \times \widetilde{\mathbf{C}}_{6\kappa'}$
- $\Sigma_4 = \left[\mathbf{O}_2(\xi^2, [0, \theta_2]) \times \mathbf{Z}_2(\delta)\right] \times \widetilde{\mathbf{C}}_{6\kappa'}$
- $\Sigma_5 = \mathbf{D}_4(\xi, \delta) \times \widetilde{\mathbf{D}}_{2\kappa}$
- $\Sigma_6 = \left[\mathbf{O}_2(\xi^2, [0, \theta_2]) \times \mathbf{Z}_2(\delta)\right] \times \widetilde{\mathbf{D}}_{2\kappa}$.

The corresponding fixed subspaces are listed in table 2.

Proof. We have already seen that $\mathbf{D}_8, \widetilde{\mathbf{C}}_{6\kappa'}$ and $\widetilde{\mathbf{D}}_{2\kappa}$ are the three axial isotropy subgroups for the irreducible representation χ_8 of $\mathcal{G}$. $\mathbf{D}_4(\xi, \delta)$ and $\mathbf{O}_2(\xi^2, [0, \theta_2]) \times \mathbf{Z}_2(\delta)$ are the two axial subgroups for the irreducible action of $\mathbf{D}_4 \ltimes \mathbb{T}^2$ on $\mathbb{C}^2$ [29, 33]. Lemma 4.7 gives the result. □

Axial subgroup	Fixed subspace
Σ_1	$\mathbb{R}\{(0,0,1,0,0,1)\}$
Σ_2	$\mathbb{R}\{(0,0,1,0,0,0)\}$
Σ_3	$\mathbb{R}\{(1,-1,1,1,-1,1)\}$
Σ_4	$\mathbb{R}\{(1,-1,1,0,0,0)\}$
Σ_5	$\mathbb{R}\{(0,1,-1,0,1,-1)\}$
Σ_6	$\mathbb{R}\{(0,1,-1,0,0,0)\}$

TABLE 2. Fixed subspaces of $\mathbb{C}^6$ for each axial subgroups.

4.6. **Selection and stability of patterns.** Close to the bifurcation point, there exists a polynomial map $\Phi(\cdot, \lambda)$ such that the change of variable:

$$V(\mathbf{r}, z) = \sum_{l=1}^{3} \left[c_l \Psi_l(z) e^{i\mathbf{k}_1 \cdot \mathbf{r}} + d_l \Psi_l(z) e^{i\mathbf{k}_2 \cdot \mathbf{r}}\right] + \sum_{l=1}^{3} \left[\bar{c}_l \Psi_l(z) e^{-i\mathbf{k}_1 \cdot \mathbf{r}} + \bar{d}_l \Psi_l(z) e^{-i\mathbf{k}_2 \cdot \mathbf{r}}\right] + \Psi(c_1, c_2, c_3, d_1, d_2, d_3, \bar{c}_1, \bar{c}_2, \bar{c}_3, \bar{d}_1, \bar{d}_2, \bar{d}_3, \lambda)$$

transforms equation (4.1) into the normal form

$$\left\{\begin{array}{rcl} \dfrac{dc_1}{dt} & = & \lambda c_1 + c_1\left[\alpha_1|c_1|^2 + \alpha_2\left(|c_2|^2+|c_3|^2\right) + \alpha_3|d_1|^2 + \alpha_4\left(|d_2|^2+|d_3|^2\right)\right] + \text{h.o.t.} \\ \dfrac{dd_1}{dt} & = & \lambda d_1 + d_1\left[\alpha_1|d_1|^2 + \alpha_2\left(|d_2|^2+|d_3|^2\right) + \alpha_3|c_1|^2 + \alpha_4\left(|c_2|^2+|c_3|^2\right)\right] + \text{h.o.t.} \end{array}\right. \tag{4.19}$$

with $(\alpha_1,\alpha_2,\alpha_3,\alpha_4)\in\mathbb{R}^4$. Equations for $\dfrac{dc_j}{dt}, \dfrac{dd_j}{dt}$, $j=2,3$, are obtained by cyclic permutation.

Proof. See appendix E for the computation of cubic equivariants. □

Remark 4.1. In order to simplify notations, we have normalized the normal form equation (4.19) such that λ is the coefficient of the linear terms and not $\frac{\lambda}{\mu_c}$ as for normal form (4.10).

Theorem 4.9. *The branches of solutions corresponding to the six maximal isotropy subgroups satisfy the following equations:*

- Σ_1 *:* $\lambda = -(\alpha_1+\alpha_3)x^2 + o(x^4)$,
- Σ_2 *:* $\lambda = -\alpha_1 x^2 + o(x^4)$,
- Σ_3 *:* $\lambda = -(\alpha_1+2\alpha_2+\alpha_3+2\alpha_4)x^2 + o(x^4)$,
- Σ_4 *:* $\lambda = -(\alpha_1+2\alpha_2)x^2 + o(x^4)$,
- Σ_5 *:* $\lambda = -(\alpha_1+\alpha_2+\alpha_3+\alpha_4)x^2 + o(x^4)$,
- Σ_6 *:* $\lambda = -(\alpha_1+\alpha_2)x^2 + o(x^4)$.

The Σ_1 branch is stable if and only if $\alpha_2+\alpha_4<\alpha_1+\alpha_3$ and $\alpha_1<-|\alpha_3|$. The Σ_2 branch is stable if and only if $\alpha_1<0$, $\alpha_2<\alpha_1$, $\alpha_3<\alpha_1$ and $\alpha_4<\alpha_1$. The Σ_3 branch is stable if and only if $\alpha_1+2\alpha_2<-|\alpha_3+2\alpha_4|$ and $\alpha_1-\alpha_2<-|\alpha_3-\alpha_4|$. The Σ_4 branch is stable if and only $\alpha_1+2\alpha_2<0$, $\alpha_1<\alpha_2$ and $\alpha_3+2\alpha_4<\alpha_1+2\alpha_2$. Branches Σ_5 and Σ_6 are never stable.

Proof. The equation of each branch of solutions comes directly from table 2 and the amplitude equations (4.19). The stability of a branch requires the computation of the Jacobian matrix of (4.19) evaluated on the branch and the study of the corresponding eigenvalues. It is always possible to set the imaginary parts of any solution $(c_1,c_2,c_3,d_1,d_2,d_3)$ to zero, by moving the origin, and then choose $(c_1,c_2,c_3,d_1,d_2,d_3)$ to be real.

For the Σ_1 branch for example, a straightforward calculation shows that the eigenvalues of the Jacobian matrix evaluated at $(0,0,x,0,0,x)$ are:

$$\begin{aligned} \mu_1 &= \lambda + 3(\alpha_1+\alpha_3)x^2 = 2(\alpha_1+\alpha_3)x^2 + o(x^4) \\ \mu_2 &= \lambda + (3\alpha_1-\alpha_3)x^2 = 2(\alpha_1-\alpha_3)x^2 + o(x^4) \\ \mu_3 &= \mu_4 = \mu_5 = \mu_6 = \lambda + (\alpha_2+\alpha_4)x^2 = (\alpha_2+\alpha_4-\alpha_1-\alpha_3)x^2 + o(x^4). \end{aligned}$$

And the stability result automatically follows. □

4.7. **Pictures of axial planforms Σ_1 and Σ_2.** We have already explained in 4.2.4 that it is possible to interpret, in term of tuning surface, planforms with $\mathbf{D}_8$-symmetry in the case of an isolated hypercolumn. This is why, we will focus only axial planforms Σ_1 and Σ_2 of theorem 4.8. For example, in the case of Σ_1, the corresponding planform can be written as:

$$a(\mathbf{r},z) = c\Psi_3(z)\left(\cos(r_1)+\sin(r_2)\right)$$

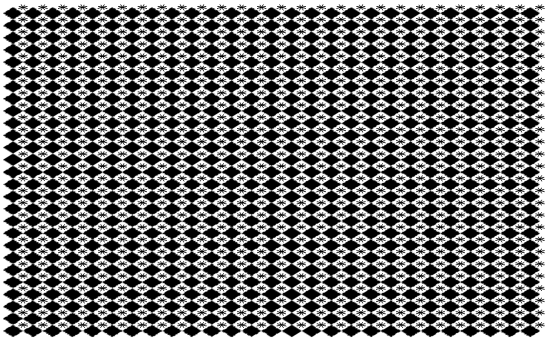

(a)

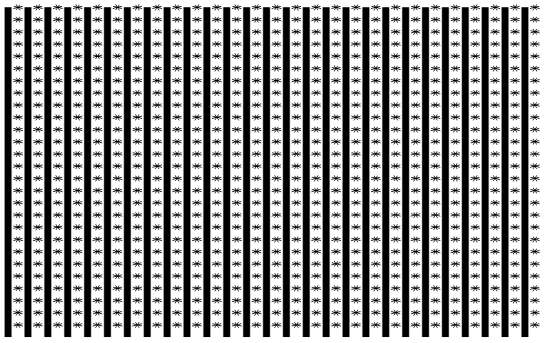

(b)

FIGURE 13. Axial eigenfunctions on the square lattice associated with $\mathbf{D}_8$-symmetry: (a) square, (b) roll.

with $\mathbf{r} = (r_1, r_2)$ and c a real constant. Planform $\Psi_3(z)$ has $z = 0$ as preferred point in the Poincaré disk such that if we further have $\cos(r_1) + \sin(r_2) > 0$ then we represent a dark region at $\mathbf{r}$ in terms of activity profile in V1 . On the other side, planform $-\Psi_3(z)$ has $z = \pm(2k+1)\pi/8$ with $k = 0 \dots 3$ as preferred points in the Poincaré disk such that when $\cos(r_1) + \sin(r_2) < 0$ we draw a star shape indicating the presence of multiple orientations at $\mathbf{r}$. In figure 13, we plot the axial planforms corresponding to square and roll solutions on the plane and $\mathbf{D}_8$ solutions on the Poincaré disk. In figures 14 and 15 we plot the planforms corresponding to branches of solution with symmetry $\gamma_1 \cdot \mathbf{D}_8$ and $\gamma_2 \cdot \mathbf{D}_8$. Note that these planforms are now contoured planforms as they only have one preferred orientation. In figures 16, 17 and 18 we plot the same planforms in the visual field coordinates, with methods developped in [14]. Planforms in figure 14 and 15 have already been found by Bressloff et al in [13, 14], whereas to our best knowledge it is the first

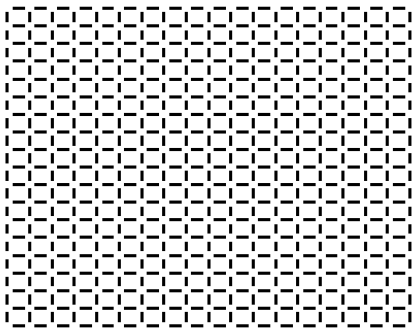

(a)

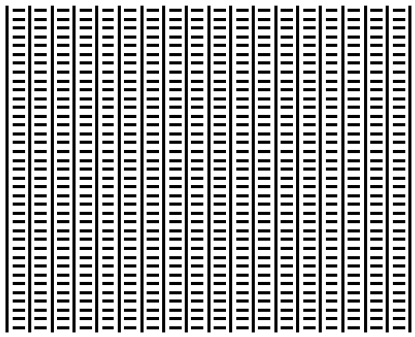

(b)

FIGURE 14. Axial eigenfunctions on the square lattice associated with $\gamma_1 \cdot \mathbf{D}_8$-symmetry: (a) square, (b) roll.

time that planform of type 13 is found. Planform in figure 13 is a combination of both contoured and non-contoured regions, contoured regions having multiple orientations. In [13, 14], contoured planforms with multiple orientations have been found only in the case of an hexagonal lattice.

4.8. **Forced symmetry breaking.** In this section we study the effect of taking $\epsilon \neq 0$ in the bifurcation problem analyzed in the previous sections. We therefore assume a square lattice in the plane and the octagonal lattice in $\mathbb{D}$. We wish to treat the problem as a weak perturbation of the isotropic case. The symmetry group when $\epsilon = 0$ is Γ and it acts as defined in (4.18). The $\mathcal{G}$ symmetry of individual hypercolumns disappears when $\epsilon \neq 0$ but something remains of it through the "shift-twist" symmetries (2.9) which act simultaneously on the "spatial" and "structure tensor" components. The action of square symmetries ξ and δ introduced in (4.18) have therefore to be replaced by the transformations $R = \xi\rho$ and $K = \delta\kappa$, which

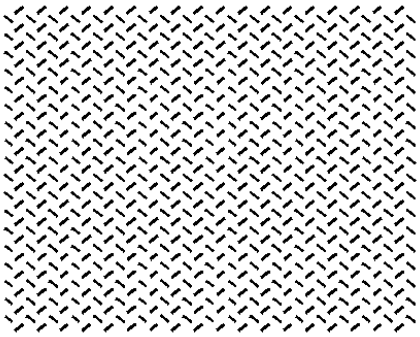

(a)

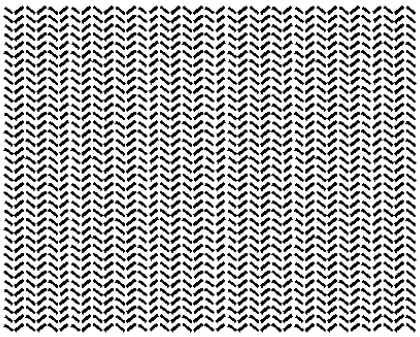

(b)

FIGURE 15. Axial eigenfunctions on the square lattice associated with $\gamma_2 \cdot \mathbf{D}_8$-symmetry: (a) square, (b) roll.

act on $(c_1, c_2, c_3, d_1, d_2, d_3)$ as follows

$$\begin{array}{rcl} R(c_1, c_2, c_3, d_1, d_2, d_3) & = & (-\bar{d}_2, \bar{d}_1, \bar{d}_3, -c_2, c_1, c_3) \\ K(c_1, c_2, c_3, d_1, d_2, d_3) & = & (-c_1, c_2, c_3, -\bar{d}_1, \bar{d}_2, \bar{d}_3) \end{array} \tag{4.20}$$

The continuous part Θ of the action in (4.18) remains unchanged. R, K and Θ define a new action of $\mathbf{D}_4 \ltimes \mathbb{T}^2$ in $\mathbb{R}^{12} \simeq \mathbb{C}^6$.

What is the effect of this perturbation on the bifurcation problem? In order to give a full description of the perturbed bifurcation diagram one should consider the codimension two bifurcation problem in the limit when both $\mu \to \mu_c$ and $\epsilon \to 0$, which requires first to compute the eigenvalues of the linear operator $\mathbf{L}_{\mu,\beta,\epsilon} = D_V \mathbf{F}(0, \mu, \beta, \epsilon)$ (see eq. (2.11) when $(\mu, \epsilon) \sim (\mu_C, 0)$. For this we need to know how the representation of $D_4 \ltimes \mathbb{T}^2$ we just defined above decomposes into irreducible components. There are two 4 dimensional irreducible representations of this group which are called scalar and pseudoscalar because the former occur naturally in the

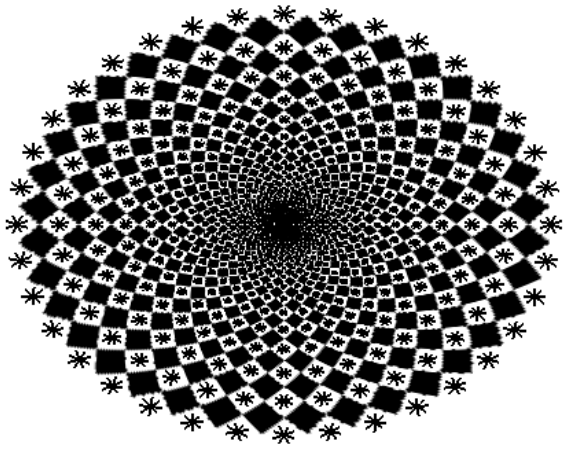

(a)

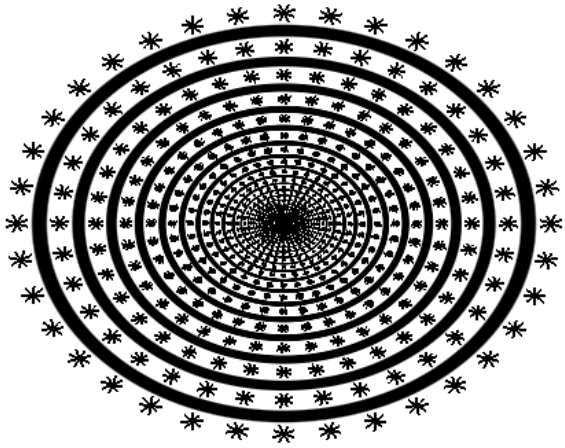

(b)

FIGURE 16. Axial eigenfunctions on the square lattice associated with $\mathbf{D}_8$-symmetry in the visual field: (a) square, (b) roll.

bifurcation analysis for scalar fields while the latter occur naturally in the analysis of pseudoscalar fields[2].

[2]A field $u : \mathbb{R}^2 \to \mathbb{R}$ is pseudoscalar if a reflection S in the plane acts by $S \cdot u(x) = -u(Sx)$), see [7]. The importance of this distinction in the context of neural fields was first noticed by [28] in the ring model.

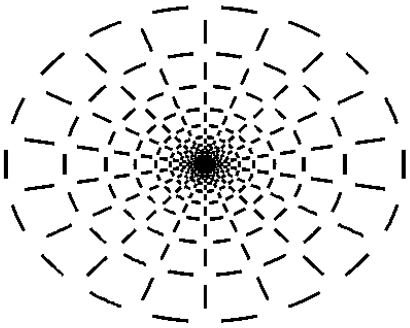

(a)

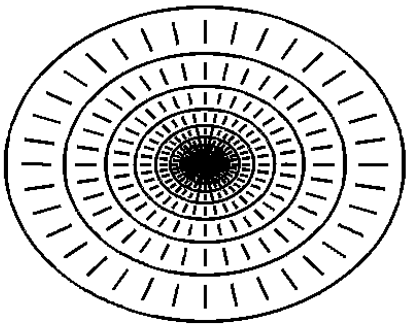

(b)

FIGURE 17. Axial eigenfunctions on the square lattice associated with $\gamma_1 \cdot \mathbf{D}_8$-symmetry in the visual field: (a) square, (b) roll.

Lemma 4.10. *The representation of* $\mathbf{D}_4 \ltimes \mathbb{T}^2$ *in* $\mathbb{R}^{12}$ *defined by* Θ *and (4.20) is the sum of three real absolutely irreducible, 4 dimensional representations* T_1, T_2, T_3, *which act respectively on the subspaces* $E_1 = \{(c_1, d_2, \bar{c}_1, \bar{d}_2)\}$, $E_2 = \{(c_2, d_1, \bar{c}_2, \bar{d}_1)\}$ *and* $E_3 = \{(c_3, d_3, \bar{c}_3, \bar{d}_3)\}$. *The representation* T_1 *is pseudoscalar while* T_2 *and* T_3 *are scalar (therefore equivalent).*

Proof. The subspaces are clearly invariant by $\Theta = [\theta_1, \theta_2]$, R and K. We note R_j and K_j the restrictions of R and K on E_j for $j = 1, 2, 3$. Then a simple computation using (4.20) shows that

$$[\pi/2, -\pi/2]\, R_2\, [-\pi/2, \pi/2] = R_3 \text{ and } [\pi/2, -\pi/2]\, K_2\, [-\pi/2, \pi/2] = K_3.$$

This implies the equivalence of T_2 and T_3. Now, T_3 is the "standard" scalar absolutely irreducible representation of dimension 4. There is however no such equivalence with T_1. Hence T_1 is the pseudoscalar irreducible representation of dimension 4. □

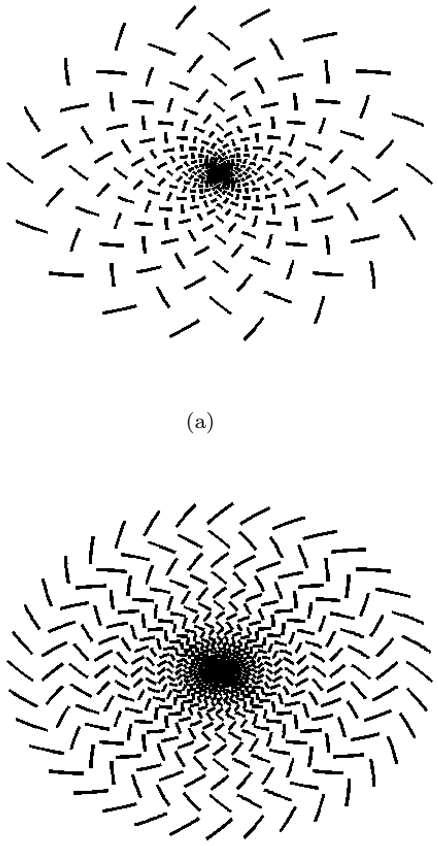

(a)

(b)

FIGURE 18. Axial eigenfunctions on the square lattice associated with $\gamma_1 \cdot \mathbf{D}_8$-symmetry in the visual field: (a) square, (b) roll.

This lemma provides the isotypic decomposition of the representation and it implies that $\mathbf{L}_{\mu,\beta,\epsilon}$ admits a bloc diagonal decomposition with one 4×4 bloc $\mathbf{L}^1_{\mu,\epsilon} = \lambda(\mu,\epsilon)\mathbf{I}_4$, $\lambda \in \mathbb{R}$ and $\lambda(0,0) = 0$, corresponding to T_1 and another 8×8 bloc $\mathbf{L}^2_{\mu,\epsilon}$ corresponding to the sum $T_2 + T_3$. We shall however not go further in this bifurcation analysis here, it will be the subject of a forthcoming work.

We can instead look at the perturbation of the branches of equilibria listed in Theorem 4.8 "far" from the bifurcation. Given such an equilibrium P, its orbit under the action of Γ consists in a disjoint union of tori which are isomorphic to $\mathbb{T}^2$, resp. $\mathbb{T}$, depending on whether its isotropy subgroup is finite, resp. contains $\mathbb{T}$. The number of connected components in the orbit is given by the action of $\mathcal{G}$, more precisely it is equal to $n_H = |\mathcal{G}|/|H|$ where H is the part in $\mathcal{G}$ of the isotropy subgroup of P. If this orbit is hyperbolic, in particular if the equilibrium is orbitally stable, it persists as an invariant set for the equation when $\epsilon \neq 0$ (small enough). Moreover this invariant set is still filled with equilibria because the torus action is

not destroyed by the perturbation. However the n_H tori are not anymore in the same group orbit and therefore they correspond to different solutions.

Let us concentrate on the solutions of types Σ_1 and Σ_2. Note that $\Gamma \cap \Sigma_1 = \Gamma \cap \Sigma_2 = \mathbf{D}_8$, hence $n_{\Sigma_1} = n_{\Sigma_2} = 96/16 = 6$. These six components correspond to the hyperbolic planforms $\pm\Psi_1(z)$, $\pm\Psi_2(z)$ and $\pm\Psi_3(z)$. These orientations persist at leading order for the perturbed equilibria.

One can say a little more. Looking for $\lambda(\mu, \epsilon) = 0$ and assuming that we have $\lambda'_\mu(0,0) \neq 0$, we have a curve of solutions $\mu_c(\epsilon)$. For a fixed value of ϵ, a bifurcation occurs at $\mu = \mu_c(\epsilon)$, with kernel E_1 and invariance by the pseudoscalar representation T_1. Therefore we expect branches of "anti-rolls" and "anti-squares" to bifurcate [7]. We recall that these planforms have isotropies $[\pi, 0]\mathbf{O}(2)$ and $[\pi, 0]\mathbf{D}_4$ respectively. Here $\mathbf{O}(2)$ is generated by the translations $[0, \theta_2]$, $\theta_2 \in S^1$, and K, while $\mathbf{D}_4$ is generated by R and K. A simple computation shows that indeed, $\dim \mathbf{Fix}([\pi, 0]\mathbf{O}(2)) = 1$ and $\dim \mathbf{Fix}([\pi, 0]\mathbf{D}_4) = 1$ (the Equivariant Branching Lemma can be applied), these axes belonging to the subspace E_1, while $\dim \mathbf{Fix}(\mathbf{O}(2)) = \dim \mathbf{Fix}(\mathbf{D}_4) = 2$ and these planes are in $E_2 + E_3$.

5. **Discussion.** In this paper we have analyzed a spatialized network of interacting hypercolumns in the context of textures perception in the primary visual cortex. Such a network is described by Wilson-Cowan neural field equations set on an abstracted cortex $\mathbb{R}^2 \times \mathbf{SPD}(2, \mathbb{R})$, where the feature space $\mathbf{SPD}(2, \mathbb{R})$ is the set of structure tensors. The coupling function of the network is characterized by local and long-range connections and can explicitly be written down. Long-range connections modulate rather than drive the cortical activity and can have an isotropic or anisotropic nature. Previous studies [18, 27] allow us to consider only structure tensors with determinant equal one and then identify the feature space to the Poincaré disk $\mathbb{D}$. We addressed two complementary problems. The first one was to study the effect of weak anisotropic lateral coupling on the cortical activity when the feature space is reduced to a bounded compact disk Ω of the Poincaré disk. The second problem that we addressed in this paper is the question of spontaneous pattern formation for a model with $\mathbf{E}(2) \times \mathbf{U}(1, 1)$ symmetry. We have restricted our study to solutions which are doubly periodic on the Euclidean plane and periodic on the Poincaré disk. The visual planforms generated by our spatialized network are correlated tuning surfaces across the visual cortex and are the counterpart of the visual geometric hallucinations for orientation in the context of textures.

Regarding the first problem, we have been able to generalized the previous results obtained by Bressloff et al [13, 14] for orientations to the context of structure tensors. We have shown that the structure tensor model, limited to a bounded compact disk Ω, is able to effectively reproduce all known planforms found in [13, 14]. In the second problem, using the symmetries of the hyperbolic octagonal lattice, we have first developed a tuning mechanism in one hypercolumn of V1 equivalent to the one used in the ring model of orientations for the Poincaré disk setting. One of the main advantage of this tuning mechanism is that both tuned (with a preferred orientation) and untuned (with no preferred orientation) responses are present within the same irreducible representation which is not the case for the ring model of orientation. Furthermore, we have made use of the concept of polar map in order to provide some neurophysiological and phenomenological evidences for such a model. We have also numerically investigated the set of parameters for which this tuning mechanism can occur. Secondly, for the spatialized network of interacting hypercolumns, we been

able to show the existence of two new planforms, which have not been identified so far with specific hallucinations (see Figures 13 and 16). These new planforms are a combination of untuned and tuned states in feature space. Note that for convenience, we have only represented the preferred orientation in each of our figures of planforms as it already gives enough information on the local structure of the visual hallucination and can be easily compare to previous studies. It would be natural to numerically investigate the set of real images that can produce such a structure tensor fields on a square lattice. This is ongoing areas of current research and will be reported on elsewhere.

In the present study, we investigated the case of spatialization with a square lattice. This choice was dictated by the fact that the octagonal lattice for the feature space is only compatible with square and rhombic lattices due to discrete rotations. The particular choice of a square lattice was somehow arbitrary but the methods developed here would naturally extend to the rhombic lattice. In order to generalize our results to a hexagonal lattice on the plane, one would have to work with a different hyperbolic lattice in the feature space which has to be compatible with $\mathbf{D}_6$-symmetry. The simplest non trivial choice of such a lattice is given by the regular hyperbolic dodecagonal lattice generated by six hyperbolic transformations which are rotated from each other by angles $k\pi/6$ ($k = 1, \ldots, 5$). The elementary polygon is now a hyperbolic dodecagon and the genus of the corresponding quotient surface is $g = 3$. Using similar techniques as the one used in [18, 26] and in this manuscript, it would be possible to analyze spontaneous pattern formation for a planar hexagonal lattice and the regular hyperbolic dodecagonal lattice which are both compatible.

As already highlighted in the introduction, a neuro-geometrical approach, adapted from Petitot, Sarti and Citti [54, 22, 58], should be developed for the structure tensor formalism. We believe that it would provide a natural extension of the neuro-geometrical theory of texture segmentation and completion problems with a biological inspired approach. It would also be interesting to see how our structure tensor formalism can be related to the image structure tensor introduced by Sarti and Citti [57] through Bragmann transform and probability measure on the set of orientations.

Another extension of our work would be to include external stimuli and see how long-range connections modulate its effects. We think that our framework (center manifold reduction close to the point of instability) is applicable if we further suppose that the external input is sufficiently weak: amplitude of order $O(\beta)$ if β is the strength of the lateral coupling function. Of course it could be interesting to include the effects of noise in our model and one approach would consist to add space-dependent noise term to the external stimuli. It will be the subject of forthcoming research.

Finally, another approach to the modeling of the primary visual cortex is to consider model with no feature space [11, 6, 2] where cortical maps are included into the equations. This requires understanding the mechanism of their formation. Wolf et al [69, 39, 38] have designed equations for the development of cortical map of orientations and Bressloff-Oster [53, 15] for ocular dominance map. One can ask the question of formation of cortical map of structure tensors during development. Then it would be very interesting to model a structure tensor map embedded in the Riemannian manifold $\mathbf{SPD}(2, \mathbb{R})$ on a growing cortex with different topology (disk, square and sphere) using an evolution equation similar to those proposed

in [39, 15]. The maps obtained from the model could be then compared to those obtained experimentally by optical imaging technics and incorporated into a model of V1 with no feature space. We plan to explore these pathes in future work.

Appendix A. **Relationships between SSPD$(2,\mathbb{R})$ and $\mathbb{D}$.** A unit determinant structure tensor $\mathcal{T}$ is a 2×2 symmetric positive definite matrix defined as

$$\mathcal{T}=\begin{pmatrix} a & c \\ c & b \end{pmatrix}$$

with $ab-c^2=1$. The corresponding point in $\mathbb{D}$ is given by:

$$z=\frac{a-b+2ic}{a+b+2} \tag{A.1}$$

where z satisfies

$$0\leq |z|=\frac{a+b-2}{a+b+2}<1.$$

Conversely given a point $z=z_1+iz_2$ representing a point of $\mathbb{D}$, the corresponding tensor coordinates are given by:

$$\begin{aligned} a&=\frac{(1+z_1)^2+z_2^2}{1-z_1^2-z_2^2}\\ b&=\frac{(1+z_1)^2-z_2^2}{1-z_1^2-z_2^2}\\ c&=\frac{2z_2}{1-z_1^2-z_2^2}. \end{aligned} \tag{A.2}$$

Note that equation (A.1) is the "**SSPD**$(2,\mathbb{R})$ to $\mathbb{D}$" dictionary that allows us to translate statements about structure tensors to statements to points in the Poincaré disk and (A.2) is the "$\mathbb{D}$ to **SSPD**$(2,\mathbb{R})$" dictionary.

Appendix B. **Isometries of the Poincaré disk.** We briefly describes the isometries of $\mathbb{D}$, i.e the transformations that preserve the distance $d_{\mathbb{D}}$. We refer to the classical textbooks in hyperbolic geometry for details, e.g, [40]. The direct isometries (preserving the orientation) in $\mathbb{D}$ are the elements of the special unitary group, noted **SU**$(1,1)$, of 2×2 Hermitian matrices with determinant equal to 1. Given:

$$\gamma=\begin{pmatrix} \alpha & \beta \\ \bar{\beta} & \bar{\alpha} \end{pmatrix} \text{ such that } |\alpha|^2-|\beta|^2=1,$$

an element of **SU**$(1,1)$, the corresponding isometry γ in $\mathbb{D}$ is defined by:

$$\gamma\cdot z=\frac{\alpha z+\beta}{\bar{\beta}z+\bar{\alpha}},\quad z\in\mathbb{D} \tag{B.1}$$

Orientation reversing isometries of $\mathbb{D}$ are obtained by composing any transformation (B.1) with the reflection $\kappa: z\to\bar{z}$. The full symmetry group of the Poincaré disc is therefore:

$$\mathbf{U}(1,1)=\mathbf{SU}(1,1)\cup\kappa\cdot\mathbf{SU}(1,1)$$

Let us now describe the different kinds of direct isometries acting in $\mathbb{D}$. We first define the following one parameter subgroups of $\mathbf{SU}(1,1)$:

$$\begin{cases} K \overset{def}{=} \{\mathrm{rot}_\phi = \begin{pmatrix} e^{i\frac{\phi}{2}} & 0 \\ 0 & e^{-i\frac{\phi}{2}} \end{pmatrix}, \phi \in \mathbb{S}^1\} \\ A \overset{def}{=} \{a_r = \begin{pmatrix} \cosh r & \sinh r \\ \sinh r & \cosh r \end{pmatrix}, r \in \mathbb{R}\} \\ N \overset{def}{=} \{n_s = \begin{pmatrix} 1+is & -is \\ is & 1-is \end{pmatrix}, s \in \mathbb{R}\} \end{cases}$$

Note that $\mathrm{rot}_\phi \cdot z = e^{i\phi} z$ and also $a_r \cdot O = \tanh r$, with O being the center of the Poincaré disk that is the point represented by $z = 0$. The group K is the orthogonal group $\mathrm{O}(2)$. Its orbits are concentric circles. It is possible to express each point $z \in \mathbb{D}$ in hyperbolic polar coordinates: $z = \mathrm{rot}_\phi a_r \cdot O = \tanh r e^{i\phi}$ and $r = d_{\mathbb{D}}(z, 0)$. The orbits of A converge to the same limit points of the unit circle $\partial\mathbb{D}$, $b_{\pm 1} = \pm 1$ when $r \to \pm\infty$. They are circular arcs in $\mathbb{D}$ going through the points b_1 and b_{-1}. The orbits of N are the circles inside $\mathbb{D}$ and tangent to the unit circle at b_1. These circles are called *horocycles* with base point b_1. N is called the horocyclic group. It is also possible to express each point $z \in \mathbb{D}$ in horocyclic coordinates: $z = n_s a_r \cdot O$, where n_s are the transformations associated with the group N ($s \in \mathbb{R}$) and a_r the transformations associated with the subgroup A ($r \in \mathbb{R}$).

Iwasawa decomposition The following decomposition holds, see [37]:

$$\mathrm{SU}(1,1) = KAN$$

This theorem allows us to decompose any isometry of $\mathbb{D}$ as the product of at most three elements in the groups, K, A and N.

Appendix C. **Computation of ϖ in 3.2.2.** We use methods developed in [31] in order to compute the coefficient ϖ in the normal form (3.7). We use the scalar product:

$$\langle \zeta_1, \zeta_j \rangle = \frac{1}{\pi} \int_0^\omega \int_0^{2\pi} \zeta_i(\tau, \theta) \zeta_j(\tau, \theta) \sinh(\tau) d\tau d\theta = \delta_{i,j}.$$

If we rewrite equation (3.4) as

$$V' = \mathbf{L}V + \mathcal{R}(V, \lambda)$$

with $\lambda = \mu - \mu_c$ and

$$\mathbf{L}V(\tau,\theta) = -V(\tau,\theta) + \mu_c s_1 \int_0^\omega \int_0^{2\pi} W_{loc}\left(\tau, \tau' \mid \theta - \theta'\right) V(\tau', \theta') \sinh(\tau') d\tau' d\theta'$$

$$\begin{aligned} \mathcal{R}(V,\lambda) = &\int_0^\omega \int_0^{2\pi} W_{loc}\left(\tau, \tau' \mid \theta - \theta'\right) S((\lambda + \mu_c) V(\tau', \theta')) \sinh(\tau') d\tau' d\theta' \\ &- \mu_c s_1 \int_0^\omega \int_0^{2\pi} W_{loc}\left(\tau, \tau' \mid \theta - \theta'\right) V(\tau', \theta') \sinh(\tau') d\tau' d\theta'. \end{aligned}$$

Taylor expanding the map Ψ:

$$\Psi(A, B, \lambda) = \sum_{1 \le s+l+m \le 3} A^s B^l \lambda^m \Psi_{slm}$$

and $\mathcal{R}$:

$$\mathcal{R}(V, \lambda) = \mathcal{R}_{11}(V, \lambda) + \mathcal{R}_{20}(V, V) + \mathcal{R}_{30}(V, V, V) + \text{h.o.t.}$$

with

$$\mathcal{R}_{11}(V,\lambda) = \lambda s_1 \int_0^\omega \int_0^{2\pi} W_{loc}\left(\tau,\tau' \mid \theta-\theta'\right) V(\tau',\theta')\sinh(\tau')d\tau' d\theta'$$
$$\mathcal{R}_{20}(U,V) = \frac{\mu_c^2 s_2}{2} \int_0^\omega \int_0^{2\pi} W_{loc}\left(\tau,\tau' \mid \theta-\theta'\right) UV(\tau',\theta')\sinh(\tau')d\tau' d\theta'$$
$$\mathcal{R}_{30}(U,V,W) = \frac{\mu_c^3 s_3}{6} \int_0^\omega \int_0^{2\pi} W_{loc}\left(\tau,\tau' \mid \theta-\theta'\right) UVW(\tau',\theta')\sinh(\tau')d\tau' d\theta'$$

where $s_2 = S''(0)$ and $s_3 = S'''(0)$ we obtain the following system of equations:

$$\begin{aligned} 0 &= \mathbf{L}\Psi_{200} + \mathcal{R}_{20}(\zeta_1,\zeta_1) \\ \varpi &= \langle 2\mathcal{R}_{20}(\Psi_{200},\zeta_1) + \mathcal{R}_{30}(\zeta_1,\zeta_1,\zeta_1),\zeta_1\rangle. \end{aligned} \tag{C.1}$$

We start by evaluating $\mathcal{R}_{20}(\zeta_1,\zeta_1)$:

$$\begin{aligned} \mathcal{R}_{20}(\zeta_1,\zeta_1) &= \frac{\mu_c^2 s_2}{2} \int_0^\omega \int_0^{2\pi} W_{loc}\left(\tau,\tau' \mid \theta-\theta'\right) \left(\mathcal{Y}_N^1(\tau')\right)^2 \cos(\theta')^2 \sinh(\tau')d\tau' d\theta' \\ &= \frac{\mu_c^2 s_2}{2}\pi \sum_{n\in\mathbb{N}^*} \mathcal{Y}_n^0(\tau)\widehat{W}_{0,n} \int_0^\omega \mathcal{Y}_n^0(\tau') \left(\mathcal{Y}_N^1(\tau')\right)^2 \sinh(\tau')d\tau' \\ &\quad + \frac{\mu_c^2 s_2}{2}\frac{\pi}{2}\cos(2\theta) \sum_{n\in\mathbb{N}^*} \mathcal{Y}_n^2(\tau)\widehat{W}_{2,n} \int_0^\omega \mathcal{Y}_n^2(\tau') \left(\mathcal{Y}_N^1(\tau')\right)^2 \sinh(\tau')d\tau' \\ &= \frac{\mu_c^2 s_2}{2} \sum_{n\in\mathbb{N}^*} \left[\pi\mathcal{Y}_n^0(\tau)\widehat{W}_{0,n}\gamma_{0,n} + \frac{\pi}{2}\cos(2\theta)\mathcal{Y}_n^2(\tau)\widehat{W}_{2,n}\gamma_{2,n}\right] \end{aligned}$$

where

$$\gamma_{k,n} = \int_0^\omega \mathcal{Y}_n^k(\tau') \left(\mathcal{Y}_1^1(\tau')\right)^2 \sinh(\tau')d\tau'.$$

This implies that:

$$\Psi_{200} = \mathrm{Span}(\zeta_1,\zeta_2) + \sum_{n\in\mathbb{N}^*} \left[c_n^0\mathcal{Y}_n^0(\tau) + c_n^2\cos(2\theta)\mathcal{Y}_n^2(\tau)\right]$$
$$\text{with} \quad c_n^0 = \frac{\mu_c^2 s_2 \pi\widehat{W}_{0,n}\gamma_{0,n}}{2\left(1-\mu_c s_1 2\pi\widehat{W}_{0,n}\right)} \text{ and } c_n^2 = \frac{\mu_c^2 s_2 \pi\widehat{W}_{2,n}\gamma_{2,n}}{4\left(1-\mu_c s_1 \pi\widehat{W}_{2,n}\right)}.$$

It is now possible to compute coefficient ϖ:

$$\begin{aligned} \langle\mathcal{R}_{20}(\Psi_{200},\zeta_1),\zeta_1\rangle &= \frac{\mu_c^2 s_2}{2}\widehat{W}_{1,1}\langle\Psi_{200},\zeta_1\zeta_1\rangle \\ &= \frac{\mu_c^4 s_2^2 \pi}{4}\widehat{W}_{1,1} \sum_{n\in\mathbb{N}^*} \left[\frac{\pi\widehat{W}_{0,n}\left(\gamma_{0,n}\right)^2}{\left(1-\mu_c s_1 2\pi\widehat{W}_{0,n}\right)} + \frac{\pi\widehat{W}_{2,n}\left(\gamma_{2,n}\right)^2}{4\left(1-\mu_c s_1 \pi\widehat{W}_{2,n}\right)}\right] \end{aligned}$$

and

$$\begin{aligned}\langle \mathcal{R}_{300}(\zeta_1,\zeta_1,\zeta_1),\zeta_1\rangle &= \frac{\mu_c^3 s_3}{6}\widehat{W}_{1,1}\langle \zeta_1\zeta_1,\zeta_1\zeta_1\rangle \\ &= \frac{\mu_c^3 s_3 \pi}{8}\widehat{W}_{1,1}\Lambda \\ \text{with} \quad \Lambda &= \int_0^\omega \left(\mathcal{Y}_1^1(\tau)\right)^4 \sinh(\tau) d\tau\end{aligned}$$

which implies

$$\varpi = \frac{\mu_c^3 \pi \widehat{W}_{1,1}}{4}\left(\frac{s_3\Lambda}{2} + \mu_c s_2^2 \sum_{n\in\mathbb{N}^*}\left[\frac{\pi\widehat{W}_{0,n}\left(\gamma_{0,n}\right)^2}{\left(1-\mu_c s_1 2\pi\widehat{W}_{0,n}\right)} + \frac{\pi\widehat{W}_{2,n}\left(\gamma_{2,n}\right)^2}{4\left(1-\mu_c s_1 \pi\widehat{W}_{2,n}\right)}\right]\right).$$

Appendix D. **Proof of Lemma 4.4.** We compute each term in the expression of a and b in (4.11).

$$\begin{aligned}\langle \mathcal{R}_{30}(\Psi_1,\Psi_3,\Psi_3),\Psi_1\rangle &= \frac{\mu_c^3 s_3}{6}\langle W_{loc}\star\left(\Psi_1\Psi_3\Psi_3\right),\Psi_1\rangle \\ &= \frac{\mu_c^3 s_3}{6}\langle \Psi_1\Psi_3\Psi_3, W_{loc}\star\Psi_1\rangle \\ &= \frac{\mu_c^3 s_3}{6}W_{loc}^c\langle \frac{1}{\sqrt{3}}\Psi_{\chi_{10}}^{\mathbf{D}'_{2\kappa}}, \frac{1}{\sqrt{3}}\Psi_{\chi_{10}}^{\mathbf{D}'_{2\kappa}}\rangle \\ &= \frac{\mu_c^3 s_3}{18}W_{loc}^c\end{aligned}$$

$$\begin{aligned}\langle \mathcal{R}_{30}(\Psi_3,\Psi_3,\Psi_3),\Psi_3\rangle &= \frac{\mu_c^3 s_3}{6}\langle W_{loc}\star\left(\Psi_3\Psi_3\Psi_3\right),\Psi_3\rangle \\ &= \frac{\mu_c^3 s_3}{6}W_{loc}^c\langle \Psi_3\Psi_3\Psi_3,\Psi_3\rangle \\ &= \frac{\mu_c^3 s_3}{6}W_{loc}^c\langle \frac{6}{5}\Psi_{\chi_6}^{\widetilde{\mathbf{D}}_{8\kappa}}(z)+1, \frac{6}{5}\Psi_{\chi_6}^{\widetilde{\mathbf{D}}_{8\kappa}}(z)+1\rangle \\ &= \frac{61\mu_c^3 s_3}{150}W_{loc}^c\end{aligned}$$

$$\begin{aligned}\langle \mathcal{R}_{20}(\Phi_{1010},\Psi_3),\Psi_1\rangle &= \frac{\mu_c^2 s_2}{2}\langle W_{loc}\star\left(\Phi_{1010}\Psi_3\right),\Psi_1\rangle \\ &= \frac{\mu_c^2 s_2}{2}W_{loc}^c\langle \Phi_{1010}\Psi_3,\Psi_1\rangle \\ &= \frac{\mu_c^4 s_2^2}{2}\frac{\widetilde{W}_{loc}^{\chi_{10},\mathbf{D}'_{2\kappa}}}{1-\widetilde{W}_{loc}^{\chi_{10},\mathbf{D}'_{2\kappa}}/\widetilde{W}_{loc}^c}W_{loc}^c\langle \frac{1}{\sqrt{3}}\Psi_{\chi_{10}}^{\mathbf{D}'_{2\kappa}}, \frac{1}{\sqrt{3}}\Psi_{\chi_{10}}^{\mathbf{D}'_{2\kappa}}\rangle \\ &= \frac{\mu_c^4 s_2^2}{6}\frac{\widetilde{W}_{loc}^{\chi_{10},\mathbf{D}'_{2\kappa}}}{1-\widetilde{W}_{loc}^{\chi_{10},\mathbf{D}'_{2\kappa}}/\widetilde{W}_{loc}^c}W_{loc}^c\end{aligned}$$

$$\begin{aligned}\langle \mathcal{R}_{20}(\Phi_{0020},\Psi_3),\Psi_3\rangle &= \frac{\mu_c^2 s_2}{2}\langle W_{loc}\star(\Phi_{0020}\Psi_3),\Psi_3\rangle\\ &= \frac{\mu_c^2 s_2}{2}W_{loc}^c\langle \Phi_{0020}\Psi_3,\Psi_3\rangle\\ &= \frac{\mu_c^4 s_2^2}{4}W_{loc}^c\left[\frac{\widetilde{W}_{loc}^{\chi_1}}{1-\widetilde{W}_{loc}^{\chi_1}/\widetilde{W}_{loc}^c}\langle\Psi_3,\Psi_3\rangle\right.\\ &\left.+\frac{\widetilde{W}_{loc}^{\chi_6,\tilde{\mathbf{D}}_{8\kappa}}}{1-\widetilde{W}_{loc}^{\chi_6,\tilde{\mathbf{D}}_{8\kappa}}/\widetilde{W}_{loc}^c}\langle\frac{6}{5}\Psi_{\chi_6}^{\tilde{\mathbf{D}}_{8\kappa}},\Psi_3^2\rangle\right]\\ &= \frac{\mu_c^4 s_2^2}{4}W_{loc}^c\left[\frac{\widetilde{W}_{loc}^{\chi_1}}{1-\widetilde{W}_{loc}^{\chi_1}/\widetilde{W}_{loc}^c}+\frac{36}{25}\frac{\widetilde{W}_{loc}^{\chi_6,\tilde{\mathbf{D}}_{8\kappa}}}{1-\widetilde{W}_{loc}^{\chi_6,\tilde{\mathbf{D}}_{8\kappa}}/\widetilde{W}_{loc}^c}\right]\end{aligned}$$

and

$$\begin{aligned}\langle \mathcal{R}_{20}(\Phi_{0020},\Psi_1),\Psi_1\rangle &= \frac{\mu_c^2 s_2}{2}\langle W_{loc}\star(\Phi_{0020}\Psi_1),\Psi_1\rangle\\ &= \frac{\mu_c^2 s_2}{2}W_{loc}^c\langle \Phi_{0020}\Psi_1,\Psi_1\rangle\\ &= \frac{\mu_c^4 s_2^2}{4}W_{loc}^c\left[\frac{\widetilde{W}_{loc}^{\chi_1}}{1-\widetilde{W}_{loc}^{\chi_1}/\widetilde{W}_{loc}^c}\langle\Psi_1,\Psi_1\rangle\right.\\ &\left.+\frac{\widetilde{W}_{loc}^{\chi_6,\tilde{\mathbf{D}}_{8\kappa}}}{1-\widetilde{W}_{loc}^{\chi_6,\tilde{\mathbf{D}}_{8\kappa}}/\widetilde{W}_{loc}^c}\langle\frac{6}{5}\Psi_{\chi_6}^{\tilde{\mathbf{D}}_{8\kappa}},\Psi_1^2\rangle\right]\\ &= \frac{\mu_c^4 s_2^2}{4}W_{loc}^c\left[\frac{\widetilde{W}_{loc}^{\chi_1}}{1-\widetilde{W}_{loc}^{\chi_1}/\widetilde{W}_{loc}^c}-\frac{2}{3}\frac{\widetilde{W}_{loc}^{\chi_6,\tilde{\mathbf{D}}_{8\kappa}}}{1-\widetilde{W}_{loc}^{\chi_6,\tilde{\mathbf{D}}_{8\kappa}}/\widetilde{W}_{loc}^c}\right]\end{aligned}$$

where $\langle\frac{6}{5}\Psi_{\chi_6}^{\tilde{\mathbf{D}}_{8\kappa}},\Psi_1^2\rangle=\langle\Psi_3^2-1,\Psi_1^2\rangle=\langle\Psi_1\Psi_3,\Psi_1\Psi_3\rangle-\langle\Psi_1,\Psi_1\rangle=\frac{1}{3}-1=-\frac{2}{3}$.

It is now a simple calculation to obtain the coefficients a and b in the reduced equation (4.10).

Appendix E. **Calculation of cubic equivariants.** We want to compute the cubic equivariants for the action group defined in (4.18). First of all, we adopt the following notations:

$$C=(c_1,c_2,c_3)\text{ and }D=(d_1,d_2,d_3)$$

such that a cubic equivariant $\mathbf{E}$ is a cubic complex polynomial of $\mathbb{C}^6$ which we write:

$$\mathbf{E}(C,D,\bar{C},\bar{D})=\begin{pmatrix}f_1(C,D,\bar{C},\bar{D})\\ f_2(C,D,\bar{C},\bar{D})\\ f_3(C,D,\bar{C},\bar{D})\\ g_1(C,D,\bar{C},\bar{D})\\ g_2(C,D,\bar{C},\bar{D})\\ g_3(C,D,\bar{C},\bar{D})\end{pmatrix}$$

It is straightforward to check that of all the possible cubic terms only $c_k|c_l|^2, c_k|d_l|^2$ and $d_k|c_l|^2, d_k|d_l|^2$ are transformed in the appropriate way by the translation $\Theta=$

$[\theta_1, \theta_2]$ such that we have:

$$f_m(C, D, \bar{C}, \bar{D}) = \sum_{k=1}^{3} c_k \sum_{l=1}^{3} \left[a_m^{kl}|c_l|^2 + b_m^{kl}|d_l|^2\right]$$
$$g_m(C, D, \bar{C}, \bar{D}) = \sum_{k=1}^{3} d_k \sum_{l=1}^{3} \left[\tilde{a}_m^{kl}|c_l|^2 + \tilde{b}_m^{kl}|d_l|^2\right]$$

with $a_m^{kl}, b_m^{kl}, \tilde{a}_m^{kl}$ and $\tilde{b}_m^{kl}$ are complex constants. Now using the reflection equivariance κ shows that:

$$-\sum_{k=1}^{3} c_k \sum_{l=1}^{3} \left[a_1^{kl}|c_l|^2 + b_1^{kl}|d_l|^2\right] = -c1 \sum_{l=1}^{3} \left[a_1^{1l}|c_l|^2 + b_1^{1l}|d_l|^2\right] + \sum_{k=2}^{3} c_k \sum_{l=1}^{3} \left[a_1^{kl}|c_l|^2 + b_1^{kl}|d_l|^2\right]$$

and

$$-\sum_{k=1}^{3} d_k \sum_{l=1}^{3} \left[\tilde{a}_1^{kl}|c_l|^2 + \tilde{b}_1^{kl}|d_l|^2\right] = -d1 \sum_{l=1}^{3} \left[\tilde{a}_1^{1l}|c_l|^2 + \tilde{b}_1^{1l}|d_l|^2\right] + \sum_{k=2}^{3} d_k \sum_{l=1}^{3} \left[\tilde{a}_1^{kl}|c_l|^2 + \tilde{b}_1^{kl}|d_l|^2\right]$$

which implies that $a_1^{kl} = b_1^{kl} = \tilde{a}_1^{kl} = \tilde{b}_1^{kl} = 0$ for all $k = 2, 3$ and $l = 1, 2, 3$ and:

$$f_1(C, D, \bar{C}, \bar{D}) = c1 \sum_{l=1}^{3} \left[a_1^{1l}|c_l|^2 + b_1^{1l}|d_l|^2\right]$$
$$g_1(C, D, \bar{C}, \bar{D}) = d1 \sum_{l=1}^{3} \left[\tilde{a}_1^{1l}|c_l|^2 + \tilde{b}_1^{1l}|d_l|^2\right].$$

Extending similar arguments for conjugate reflections of κ we finally have:

$$f_m(C, D, \bar{C}, \bar{D}) = c_m \sum_{l=1}^{3} \left[a_m^{ml}|c_l|^2 + b_m^{ml}|d_l|^2\right]$$
$$g_m(C, D, \bar{C}, \bar{D}) = d_m \sum_{l=1}^{3} \left[\tilde{a}_m^{ml}|c_l|^2 + \tilde{b}_m^{ml}|d_l|^2\right].$$

Now using reflection equivariance Δ and $\xi^2\Delta$ leads to the requirement that a_m^{ml}, b_m^{ml}, $\tilde{a}_m^{ml}$ and $\tilde{b}_m^{ml}$ are real. The rotation equivariance ξ imposes the conditions that:

$$a_m^{ml} = \tilde{b}_m^{ml} \text{ and } b_m^{ml} = \tilde{a}_m^{ml}.$$

This reduces the form the equivariant map $\mathbf{E}$ to:

$$f_m(C, D, \bar{C}, \bar{D}) = c_m \sum_{l=1}^{3} \left[a_m^{ml}|c_l|^2 + b_m^{ml}|d_l|^2\right]$$
$$g_m(C, D, \bar{C}, \bar{D}) = d_m \sum_{l=1}^{3} \left[b_m^{ml}|c_l|^2 + a_m^{ml}|d_l|^2\right]$$

with real coefficients. To conclude the computation, we use the result about cubic equivariants with octahedral symmetry [47] that we used for the normal form in equation (3.7) (equivariance with respect to ρ, σ and ϵ) and find that the following conditions have to be satisfied:

$$\begin{aligned}
a_1^{11} &= a_2^{22} = a_3^{33} \\
b_1^{11} &= b_2^{22} = b_3^{33} \\
a_1^{12} &= a_1^{13} = a_2^{21} = a_2^{23} = a_3^{31} = a_3^{32} \\
b_1^{12} &= b_1^{13} = b_2^{21} = b_2^{23} = b_3^{31} = b_3^{32}.
\end{aligned}$$

This gives:

$$\mathbf{E}(C,D,\bar{C},\bar{D}) = \begin{pmatrix}
c_1\left[\alpha_1|c_1|^2 + \alpha_2\left(|c_2|^2+|c_3|^2\right) + \alpha_3|d_1|^2 + \alpha_4\left(|d_2|^2+|d_3|^2\right)\right] \\
c_2\left[\alpha_1|c_2|^2 + \alpha_2\left(|c_1|^2+|c_3|^2\right) + \alpha_3|d_2|^2 + \alpha_4\left(|d_1|^2+|d_3|^2\right)\right] \\
c_3\left[\alpha_1|c_3|^2 + \alpha_2\left(|c_1|^2+|c_2|^2\right) + \alpha_3|d_3|^2 + \alpha_4\left(|d_2|^2+|d_1|^2\right)\right] \\
d_1\left[\alpha_1|d_1|^2 + \alpha_2\left(|d_2|^2+|d_3|^2\right) + \alpha_3|c_1|^2 + \alpha_4\left(|c_2|^2+|c_3|^2\right)\right] \\
d_2\left[\alpha_1|d_2|^2 + \alpha_2\left(|d_1|^2+|d_3|^2\right) + \alpha_3|c_2|^2 + \alpha_4\left(|c_2|^2+|c_3|^2\right)\right] \\
d_3\left[\alpha_1|d_3|^2 + \alpha_2\left(|d_2|^2+|d_1|^2\right) + \alpha_3|c_3|^2 + \alpha_4\left(|c_2|^2+|c_1|^2\right)\right]
\end{pmatrix}$$

with $(\alpha_1,\alpha_2,\alpha_3,\alpha_4) \in \mathbb{R}^4$.

Acknowledgements. We would like to thank the referees very much for their valuable comments and suggestions.

REFERENCES

[1] R. Aurich and F. Steiner. *Periodic-orbit sum rules for the hadamard-gutzwiller model.* Physica D, 39:169–193, 1989.

[2] T.I. Baker and J.D. Cowan. *Spontaneous pattern formation and pinning in the primary visual cortex.* Journal of Physiology-Paris, 103(1-2):52–68, 2009.

[3] N.L. Balazs and A. Voros. *Chaos on the pseudosphere.* Physics Reports, 143(3):109–240, 1986.

[4] R. Ben-Yishai, RL Bar-Or, and H. Sompolinsky. *Theory of orientation tuning in visual cortex.* Proceedings of the National Academy of Sciences, 92(9):3844–3848, 1995.

[5] J. Bigun and G. Granlund. *Optimal orientation detection of linear symmetry.* In Proc. First Int'l Conf. Comput. Vision, pages 433–438. EEE Computer Society Press, 1987.

[6] B. Blumenfeld, D. Bibitchkov and M. Tsodyks *Neural network model of the primary visual cortex: from functional architecture to lateral connectivity and back* Journal of Computational Neuroscience, 20:219–241, 2006.

[7] I. Bosch Vivancos, P. Chossat and I. Melbourne *New planforms in systems of partial differential equations with Euclidean symmetry* Archive for rational mechanics and analysis,131(3) 199–224, 1995.

[8] W.H. Bosking, Y. Zhang, B. Schofield, and D. Fitzpatrick. *Orientation selectivity and the arrangement of horizontal connections in tree shrew striate cortex.* The Journal of Neuroscience, 17(6):2112–2127, 1997.

[9] P. C. Bressloff and J. D.Cowan. *The functional geometry of local and horizontal connections in a model of v1.* Journal of Physiology, Paris, 97:221–236, 2003.

[10] P. C. Bressloff and J. D. Cowan. *A spherical model for orientation and spatial frequency tuning in a cortical hypercolumn.* Philosophical Transactions of the Royal Society B, 2003.

[11] P.C. Bressloff. *Spatially periodic modulation of cortical patterns by long-range horizontal connections.* Physica D: Nonlinear Phenomena, 185(3-4):131–157, 2003.

[12] P.C. Bressloff and J.D. Cowan. *The visual cortex as a crystal.* Physica D: Nonlinear Phenomena, 173(3–4):226–258, December 2002.

[13] P.C. Bressloff, J.D. Cowan, M. Golubitsky, and P.J. Thomas. *Scalar and pseudoscalar bifurcations motivated by pattern formation on the visual cortex.* Nonlinearity, 14:739, 2001.

[14] P.C. Bressloff, J.D. Cowan, M. Golubitsky, P.J. Thomas, and M.C. Wiener. *Geometric visual hallucinations, euclidean symmetry and the functional architecture of striate cortex.* Phil. Trans. R. Soc. Lond. B, 306(1407):299–330, March 2001.

[15] P.C. Bressloff and A.M. Oster. *Theory for the alignment of cortical feature maps during development.* Physical Review E , 82, 021920, 2010.
[16] I. Chavel. "Eigenvalues in Riemannian Geometry", volume 115. Academic Press, 1984.
[17] S. Chemla and F. Chavane. *Voltage-sensitive dye imaging: Technique review and models.* Journal of Physiology-Paris, 104(1-2):40–50, 2010.
[18] P. Chossat, G. Faye, and O. Faugeras. *Bifurcations of hyperbolic planforms.* Journal of Nonlinear Science, February 2011.
[19] P. Chossat and R. Lauterbach. "Methods in Equivariant Bifurcations and Dynamical Systems". World Scientific Publishing Company, Singapur, 2000.
[20] P. Chossat and O. Faugeras. *Hyperbolic planforms in relation to visual edges and textures perception.* Plos Comput Biol, 5(12):e1000625, December 2009.
[21] P.G. Ciarlet and J.L. Lions, editors. "Handbook of Numerical Analysis". Volume II. Finite Element Methods (part1). North-Holland, 1991.
[22] G. Citti and A. Sarti. *A Cortical Based Model of Perceptual Completion in the Roto-Translation Space.* J Math Imaging Vis, pp. 307–326, 2006.
[23] D.P. Edwards, K.P. Purpura and E. Kaplan. *Contrast sensitivity and spatial frequency response of primate cortical neurons in and around the cytochrome oxidase blobs.* Vision Research, vol. 35, pages 1501–1523, 1995.
[24] I. Erdélyi. "Higher Transcendental Functions", volume 1. Robert E. Krieger Publishing Company, 1985.
[25] GB Ermentrout and JD Cowan. *A mathematical theory of visual hallucination patterns.* Biological Cybernetics, 34(3):137–150, 1979.
[26] G. Faye and P. Chossat. *Bifurcation diagrams and heteroclinic networks of octagonal h-planforms.* Journal of Nonlinear Science, 22(1):277–326 , 2012.
[27] G. Faye, P. Chossat, and O. Faugeras. *Analysis of a hyperbolic geometric model for visual texture perception.* The Journal of Mathematical Neuroscience, 1(4), 2011.
[28] M. Golubitsky, L.J. Shiau, and A. Török. *Bifurcation on the visual cortex with weakly anisotropic lateral coupling.* SIAM Journal on Applied Dynamical Systems, 2(2):97–143, 2003.
[29] M. Golubitsky, I. Stewart, and D.G. Schaeffer. "Singularities and Groups in Bifurcation Theory", volume II. Springer, 1988.
[30] D. Hansel and H. Sompolinsky. *Modeling feature selectivity in local cortical circuits.* Methods of Neuronal Modeling, pages 499–567, 1997.
[31] M. Haragus and G. Iooss. "Local bifurcations, center manifolds, and normal forms in infinite dimensional systems". EDP Sci. Springer Verlag UTX series, 2010.
[32] S. Helgason. "Groups and Geometric Analysis", volume 83 of *Mathematical Surveys and Monographs*. American Mathematical Society, 2000.
[33] R.B. Hoyle. "Pattern Formation: an Introduction to Methods". Cambridge Univ Pr, 2006.
[34] D.H. Hubel and T.N. Wiesel. *Receptive fields and functional architecture in two nonstriate visual areas (18 and 19) of the cat.* Journal of Neurophysiology, 28:229–289, 1965.
[35] D.H. Hubel and T.N. Wiesel. *Receptive fields and functional architecture of monkey striate cortex.* The Journal of Physiology, 195(1):215, 1968.
[36] D.H. Hubel and T.N. Wiesel. *Functional architecture of macaque monkey.* Proceedings of the Royal Society, London [B]: 1–59, 1977.
[37] H. Iwaniec. "Spectral methods of automorphic forms", volume 53 of *AMS Graduate Series in Mathematics*. AMS Bookstore, 2002.
[38] M. Kaschube, M. Schnabel, S. Löwel, D.M. Coppola, L.E. White, and F. Wolf. *Universality in the evolution of orientation columns in the visual cortex.* Science, 330(6007):1113, 2010.
[39] M. Kaschube, M. Schnabel, and F. Wolf. *Self-organization and the selection of pinwheel density in visual cortical development.* New Journal of Physics, 10:015009, 2008.
[40] S. Katok. "Fuchsian Groups". Chicago Lectures in Mathematics. The University of Chicago Press, 1992.
[41] H. Kluver. "Mescal, and mechanisms of hallucinations". University of Chicago Press Chicago, 1966.
[42] H. Knutsson. *Representing local structure using tensors.* Scandinavian Conference on Image Analysis, pages 244–251, 1989.
[43] N.N. Lebedev. "Special functions and their applications" (edited by R.A. Silverman). Dover Pubns, 1972.

[44] P.S. Leon, I. Vanzetta, G.S. Masson and L.U. Perrinet. *Motion Clouds: Model-based stimulus synthesis of natural-like random textures for the study of motion perception.* Journal of Neurophysiology, 107(11), pp. 3217-3.226, 2012

[45] M.S. Livingstone and D.H. Hubel. *Anatomy and physiology of a color system in the primate visual cortex.* Journal of Neuroscience, vol. 4, pages 309—356, 1984.

[46] J. S. Lund, A. Angelucci, and P. C. Bressloff. *Anatomical substrates for functional columns in macaque monkey primary visual cortex.* Cerebral Cortex, 12:15–24, 2003.

[47] I. Melbourne. *A singularity theory analysis of bifurcation problems with octahedral symmetry.* Dynamics and Stability of Systems, Vol. 1, No. 4, 1986.

[48] W. Miller. "Symmetry groups and their applications". Academic Press, 1972.

[49] M. Moakher. *A differential geometric approach to the geometric mean of symmetric positie-definite matrices.* SIAM J. Matrix Anal. Appl., vol 26, no 3, pp. 735-747, 2005.

[50] J.D. Murray. "Mathematical Biology II, Spatial Models and Biomedical Applications". Springer, 2003.

[51] G.A. Orban, H. Kennedy, and J. Bullier. *Velocity sensitivity and direction selectivity of neurons in areas V1 and V2 of the monkey: influence of eccentricity.* Journal of Neurophysiology, 56(2):462–480, August 1986.

[52] G. Oster. *Phosphenes.* Scientific American, 222(2):82, 1970.

[53] A.M. Oster and P.C. Bressloff. *A Developmental Model of Ocular Dominance Column Formation on a Growing Cortex.* Bulletin of Mathematical Biology, DOI 10.1007/s11538-005-9055-7, 2006.

[54] J. Petitot. *The neurogeometry of pinwheels as a sub-Riemannian contact structure.* Journal of Physiology-Paris, vol. 97, no. 2-3, pages 265–309, 2003.

[55] J. Petitot. "Neurogéométrie de la Vision". Les Éditions de l'École polytechnique, 2009.

[56] G. Sanguinetti, A. Sarti and G. Citti. *Implementation of a Model for Perceptual Completion in* $\mathbb{R}^2 \times S^1$. Computer vision and computer graphics, Communications in Computer and Information Science, Volume 24, pp.188–201, 2009.

[57] A. Sarti and G. Citti. *Non-commutative field theory in the visual cortex.* Computer Vision: from surfaces to 3D objects, C. Tyler editor, CRC Press, 2010.

[58] A. Sarti, G. Citti and J. Petitot. *The symplectic structure of the primary visual cortex.* Biological Cybernetics, vol. 98, no. 1, pages 33–48, 2008.

[59] J. Schummers, J. Mariño, and M. Sur. *Synaptic integration by v1 neurons depends on location within the orientation map.* Neuron, 36(5):969–978, 2002.

[60] J.P. Serre. "Représentations Linéaires des Groupes Finis". Hermann, 1978.

[61] L.C. Sincich and J.C. Horton. *Divided by cytochrome oxidase: A map of the projections from V1 to V2 in macaques.* Science, vol. 295, pages 1734—1737, 2002.

[62] A. Terras. "Harmonic analysis on symmetric spaces and applications", volume 2. Springer-Verlag, 1988.

[63] R.B.H. Tootell, S.L. Hamilton, M.S. Silverman, E. Switkes and R.L. De Valois. *Functional anatomy of macaque striate cortex. V. Spatial Frequency.* Journal of Neuroscience, vol. 8, pages 1610—1624, 1988.

[64] R. Veltz and O. Faugeras. *Local/global analysis of the stationary solutions of some neural field equations.* SIAM Journal on Applied Dynamical Systems, 2010.

[65] R. Veltz and O. Faugeras. *Illusions in the ring model of visual orientation selectivity.* Technical report, arXiv, 2010.

[66] G.N. Watson. "A treatise on the theory of Bessel functions". Cambridge University Press, 1995.

[67] H.R. Wilson and J.D. Cowan. *Excitatory and inhibitory interactions in localized populations of model neurons.* Biophys. Journal, 12:1–24, 1972.

[68] H.R. Wilson and J.D. Cowan. *A mathematical theory of the functional dynamics of cortical and thalamic nervous tissue.* Biological Cybernetics, 13(2):55–80, September 1973.

[69] F. Wolf and T. Geisel. *Spontaneous pinwheel annihilation during visual development.* Nature, 395(6697):73–78, 1998.

[70] A. Zettl. "Sturm-Liouville Theory", volume 121. American Mathematical Society, 2005.

E-mail address: gfaye@umn.edu
E-mail address: chossat@unice.fr